

Leptogenesis and neutrino mass with scalar leptoquarks

Kåre Fridell^{a,b}

^a*Theory Center, Institute of Particle and Nuclear Studies,
High Energy Accelerator Research Organization (KEK), Tsukuba 305-0801, Japan*

^b*Department of Physics, Florida State University, Tallahassee, FL 32306, USA*

E-mail: karef@post.kek.jp

ABSTRACT: Leptoquarks are known to generate a wide range of potentially observable phenomena, and have been searched for in different experiments. We show that the observed baryon asymmetry and neutrino mass scale can both be simultaneously produced in a model featuring scalar leptoquarks while avoiding existing experimental constraints and potentially leading to future observable signatures.

Contents

1	Introduction	1
2	The model	2
3	Leptogenesis	5
4	Phenomenology	8
4.1	Colliders	9
4.2	Neutrinoless double beta decay	9
4.3	Rare kaon decays	9
4.4	Baryon number violation	10
4.5	Flavour violation	11
5	Results	12
6	Conclusion	16
A	Boltzmann equations	17

1 Introduction

The origin of the observed asymmetry between matter and antimatter in the Universe is a long-standing problem of particle physics. From measurements of the cosmic microwave background (CMB) we know that this asymmetry is relatively small [1],

$$\eta_B^{\text{obs}} = (6.20 \pm 0.15) \times 10^{-10} \quad (1.1)$$

at 68% C.L., where $\eta_B \equiv n_B/n_\gamma$ is the number density of baryons n_B normalized to that of photons n_γ , yet how it is generated is unknown. For the asymmetry to be dynamically generated the underlying theory must violate the conservation of baryon number B .

Another unsolved problem of particle physics is the origin of neutrino masses m_ν . From observations of neutrino oscillations [2, 3] we know that at least two neutrino mass eigenstates are non-zero, yet the mechanism behind neutrino mass generation remains unknown. For pure Dirac neutrinos the corresponding Yukawa couplings y_ν must be very small, $y_\nu \sim 10^{-12}$. Another alternative is that neutrinos are Majorana particles, in which case their corresponding mass term violates the conservation of lepton number L .

Sphaleron interactions violate the conservation of $B+L$, the sum of baryon- and lepton numbers, and are predicted to be active in the early Universe [4]. Any theory that only violates L can therefore indirectly lead to B violation via the sphaleron interactions. This

fact, together with the observation that both η_B and $m_\nu/\Lambda_{\text{EWSB}}$ are very small numbers (where Λ_{EWSB} is the scale of electroweak symmetry breaking), may suggest that the generation of neutrino masses and the baryon asymmetry of the Universe (BAU) could have a common origin in a process known as leptogenesis.

One such scenario is the type-I seesaw model [5–8], in which the right-handed neutrinos N have a Majorana mass term $m_N \gtrsim 10^9$ GeV [9]. This model can accommodate the observed neutrino mass spectrum without invoking extremely small couplings, and can lead to the generation of a BAU via standard leptogenesis [10], i.e. the out-of-equilibrium decay of N into a lepton- and Higgs doublet pair. One drawback with this model is that it is difficult to observe experimentally due to the high mass scale of N , and the fact that its only interaction with the SM is via the Yukawa coupling to the Higgs. The scale m_N can be lowered e.g. in models of resonant leptogenesis [11], but this relies on a very small mass splitting between the different generations of N .

At the same time, we know that there exists a class of radiative neutrino mass models in which the Majorana masses are generated at e.g. 1-loop order [12–15] (see Ref. [16] for a review). If the fermion running in the loop is a quark the corresponding bosonic mediator would be a leptoquark [17–25]. Leptoquark models lead to several distinct observables apart from neutrino mass generation [26–28], and can potentially lead to leptogenesis [29–33]. However, it has remained unknown whether leptoquarks can simultaneously lead to the generation of neutrino masses and the observed BAU. In Ref. [33] leptoquarks were shown to potentially lead to the leptogenesis via scattering, but the corresponding neutrino mass scale was found to be too large by several orders of magnitude. However, the model in Ref. [33] could still lead to the observed neutrino mass spectrum via cancellations from other neutrino mass contributions.

In this work, we show that neutrino masses and leptogenesis via decay can both be simultaneously generated without special cancellations in a model featuring scalar leptoquarks. This result relies on the consistent treatment of $\Delta L = 2$ washout channels, for which we find that the corresponding reaction rate is proportional to the size of the neutrino mass.

In Sec. 2 we describe the model and neutrino mass generation mechanism, and in Sec. 3 we describe the leptogenesis mechanism, while the corresponding details are shown in Appendix A. In Sec. 4 we discuss different phenomenological constraints, and in Sec. 5 we show our results. We conclude in Sec. 6.

2 The model

The model that we consider consists of an extension of the Standard Model (SM) field content by three scalar leptoquarks: $S_1 \in (\bar{3}, 1, 1/3)$, $\tilde{R}_2 \in (3, 2, 1/6)$, and $S_3 \in (\bar{3}, 3, 1/3)$. The Lagrangian is (c.f. Ref. [34])

$$\begin{aligned} \mathcal{L} = & \mathcal{L}_{\text{SM}} - \tilde{R}_2^\dagger (\square + m_{\tilde{R}_2}^2) \tilde{R}_2 - S_1^* (\square + m_{S_1}^2) S_1 - S_3^{a\dagger} (\square + m_{S_3}^2) S_3^a - \lambda_1 v_{B-L} S_1 H^\dagger \tilde{R}_2 \\ & - \lambda_3 v_{B-L} H^\dagger \sigma^a S_3^a \tilde{R}_2 - g_2^{ij} \bar{L}_i i \sigma_2 \tilde{R}_2^\dagger d_j - g_1^{ij} \bar{Q}_i^c i \sigma_2 L_j S_1 - g_3^{ij} \bar{Q}_i^c i \sigma_2 \sigma^a S_3^a L_j + \text{h.c.} \end{aligned} \quad (2.1)$$

Field	Representation
H	$S(1, 2, 1/2)(0, 0)$
L	$F_L(1, 2, -1/2)(0, 1)$
\bar{e}^c	$F_R(1, 1, -1)(0, 1)$
Q	$F_L(3, 2, 1/6)(1, 0)$
\bar{u}^c	$F_R(3, 1, 2/3)(1, 0)$
\bar{d}^c	$F_R(3, 1, -1/3)(1, 0)$
S_1	$S(\bar{3}, 1, 1/3)(-1, -1)$
\tilde{R}_2	$S(3, 2, 1/6)(1, -1)$
S_3	$S(\bar{3}, 3, 1/3)(-1, -1)$

Table 1: Field content of the model described by the Lagrangian in Eq. (2.1). The second column shown the representation under the SM gauge group, where S and $F_{L(R)}$ denote a scalar and left- (right-) handed fermion field, respectively. The last parenthesis shows $(3B, L)$ where B is the baryon number and L the lepton number.

Here $\square = \eta^{\mu\nu} \partial_\mu \partial_\nu$ is the d'Alembert operator. The representations under the SM gauge group $SU(3)_c \times SU(2)_L \times U(1)_Y$ of the different fields, as well as their Lorentz structure, are shown in Tab. 1, where S and $F_{L(R)}$ denote a scalar and left- (right-) handed fermion field, respectively, and the last parenthesis shows $(3B, L)$, where B and L are the baryon- and lepton numbers, respectively. Note that both S_1 and S_3 can have additional couplings to the SM fermions not included in Eq. (2.1), we have omitted them since they are not directly involved in the leptogenesis mechanism. We have also considered a scenario where the tri-scalar couplings $\lambda_1 v_{B-L}$ and $\lambda_3 v_{B-L}$ are generated by the same $B - L$ -breaking vacuum expectation value (VEV) v_{B-L} . This was done for simplicity but does not represent the most general scenario. All three leptoquarks are assigned a lepton number $L = -1$, while S_1 and S_3 have baryon number $B = -1/3$ and \tilde{R}_2 has $B = 1/3$. With this assignment the two tri-scalar couplings in Eq. (2.1) violate lepton number by two units, $\Delta L = 2$, and can therefore potentially lead to Majorana neutrino masses and the generation of a BAU via leptogenesis.

We consider the mass hierarchy $m_{S_3} > m_{S_1} \gg m_{\tilde{R}_2} \gg \Lambda_{\text{EWSB}}$. At low energies this leads to an effective Lagrangian [35–40]

$$\mathcal{L}_{\text{eff}} = C_{\bar{d}LQLH1}^{prst} \mathcal{O}_{\bar{d}LQLH1}^{prst} + C_{\bar{d}LQLH2}^{prst} \mathcal{O}_{\bar{d}LQLH2}^{prst} + \text{h.c.} \quad (2.2)$$

with two dimension-7 $\Delta L = 2$ operators

$$\mathcal{O}_{\bar{d}LQLH1}^{prst} = \epsilon_{ij} \epsilon_{mn} (\bar{d}_p L_r^i) (\bar{Q}_s^{cj} L_t^m) H^n, \quad \mathcal{O}_{\bar{d}LQLH2}^{prst} = \epsilon_{im} \epsilon_{jn} (\bar{d}_p L_r^i) (\bar{Q}_s^{cj} L_t^m) H^n. \quad (2.3)$$

These operators will lead to a number of potentially observable low-energy phenomena, as discussed in Sec. 4. The Wilson coefficients are generated by the model parameters for both S_1 and S_3 . However, since we consider the hierarchy $m_{S_3} > m_{S_1}$, the dominant contribution will come from S_1 , and we therefore neglect the S_3 component of the Wilson coefficients,

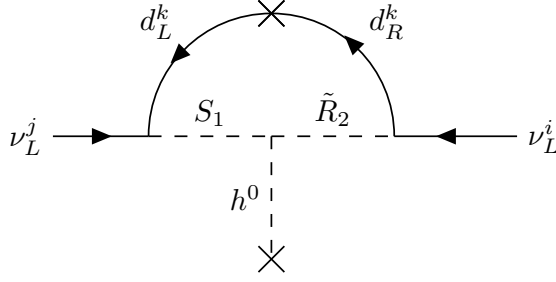


Figure 1: Radiative neutrino mass generated by the model described in the text.

such that

$$C_{dLQLH1}^{prst} = -\frac{\lambda_1 v_{B-L} g_1^{ps} g_2^{rt}}{m_{\tilde{R}_2}^2 m_{S_1}^2}, \quad C_{dLQLH2}^{ijkn} = \frac{\lambda_1 v_{B-L} g_1^{ps} g_2^{rt}}{m_{\tilde{R}_2}^2 m_{S_1}^2}. \quad (2.4)$$

Upon electroweak symmetry breaking the component of \tilde{R}_2 with hypercharge $Q = -1/3$ will mix with both S_1^* and the $Q = -1/3$ component of S_3^\dagger via the two tri-scalar couplings to the SM Higgs. However, since we consider the mass hierarchy $m_{S_3} > m_{S_1}$, we expect that the main contribution to the neutrino mass will come from the mixing of \tilde{R}_2 with S_1 rather than S_3 . The presence of S_3 is still a crucial component of the model, since without it there would be no CP -violation in the decays of S_1 during the leptogenesis mechanism (c.f. Sec. 3). This role could also be filled by another leptoquark, such as a second copy of S_1 , and we have here chosen S_3 as an example. Note that S_1 and S_3 can also mix at 1-loop level, but we neglect this effect here due to the smallness of this mixing (c.f. Sec. 3). Considering only the S_1 contribution we have the neutrino mass matrix [19, 20, 22]

$$(m_\nu)_{ij} = \frac{3 \sin(2\theta) v (g_1^T \cdot y^d \cdot g_2 + g_2^T \cdot y^d \cdot g_1)_{ij}}{32\pi^2} \log \frac{m_{LQ_1}^2}{m_{LQ_2}^2}, \quad (2.5)$$

where the mixing angle θ is given by

$$\tan(2\theta) = \frac{2\lambda_1 v_{B-L} v}{m_{\tilde{R}_2}^2 - m_{S_1}^2}, \quad (2.6)$$

and the mass eigenstates $m_{LQ_{1,2}}$ by

$$m_{LQ_{1,2}}^2 = \frac{1}{2} \left(m_{\tilde{R}_2}^2 + m_{S_1}^2 \pm \sqrt{(m_{\tilde{R}_2}^2 - m_{S_1}^2)^2 + 4\lambda_1^2 v_{B-L}^2 v^2} \right). \quad (2.7)$$

The corresponding radiative neutrino mass diagram is shown in Fig. 1. Note that a large hierarchy of scales $m_{S_1} \gg m_{\tilde{R}_2}$ leads to a neutrino mass expression that is mostly independent of the smaller mass $m_{\tilde{R}_2}$ [41]. Eq. (2.5) can be diagonalized using the Pontecorvo–Maki–Nakagawa–Sakata (PMNS) matrix U such that $\hat{m}_\nu = U^\dagger (m_\nu)_{ij} U$, where \hat{m}_ν is diagonal. In subsequent sections we neglect CP -violation in the lepton mixing by taking U to be real. To find the model parameters that lead to the observed neutrino mass scale $m_\nu \sim \text{Tr}(\hat{m}_\nu)$ we use the central values of the normal ordering mixing angles and mass

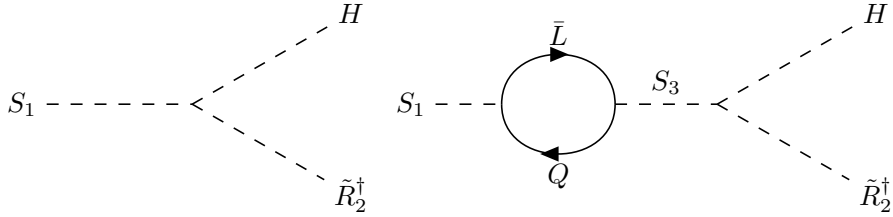


Figure 2: Tree-level- and 1-loop decay diagrams leading to CP -violation.

splittings from NUFIT v6.0 [42]. The minimum value for m_ν is then chosen as the case where the smallest neutrino mass scale m_1 vanishes $m_1 \rightarrow 0$, where $\hat{m}_\nu = \text{diag}(m_1, m_2, m_3)$. For the largest allowed neutrino mass scale we use the result $\sqrt{\sum_i |U_{ei}|^2 \hat{m}_i^2} < 0.45$ eV at 90% C.L. from the KATRIN experiment [43] and solve for m_1 . With this method we find the upper limit $m_1 < 0.30$ eV. Due to its model-independent nature, we choose to use the ground-based KATRIN constraint rather than the more stringent limit $\text{Tr}(\hat{m}) < 0.12$ eV at 95% C.L. coming from observations of the CMB by Planck [1].

In addition to the neutrino mass contribution in Eq. (2.5), the model could accommodate right-handed neutrinos and subsequently generate a Dirac mass term or an additional Majorana contribution via the type-I seesaw mechanism. In fact, S_1 could have tree-level couplings to right-handed neutrinos and down-type quark singlets. We do not include this possibility here.

3 Leptogenesis

The model described in Sec. 2 has the potential to lead to a baryon asymmetry of the Universe if the three Sakharov conditions [44]

1. B -violation
2. C - and CP -violation
3. Out-of-equilibrium dynamics

are fulfilled. The SM fermion fields are not chirally symmetric and therefore already violate C symmetry. Furthermore, the SM electroweak sphaleron interactions violate $B + L$ symmetry but rapidly reach equilibrium in the early Universe [45, 46] and cannot source a BAU on their own.

In our scheme the BAU is generated via $\Delta L = 2$ out-of-equilibrium $S_1 \rightarrow H \tilde{R}_2^\dagger$ decays. We ignore the dynamics of S_3 since its mass is greater than that of S_1 , and its abundance has therefore presumably decayed away before the onset of S_1 decays. Note however that S_3 is still needed for successful leptogenesis due to its contribution to loop-level S_1 decays, leading to CP -violation. We further neglect thermal effects such as thermal masses and thermal corrections to decays, scattering processes, and CP -asymmetries (see e.g. Ref. [47]). The CP -violation in our mechanism comes from the interference between tree- and loop-level decay diagrams of S_1 shown in Fig. 2. Note that there is also CP -violation in $S_1 \rightarrow \bar{L} \bar{Q}$

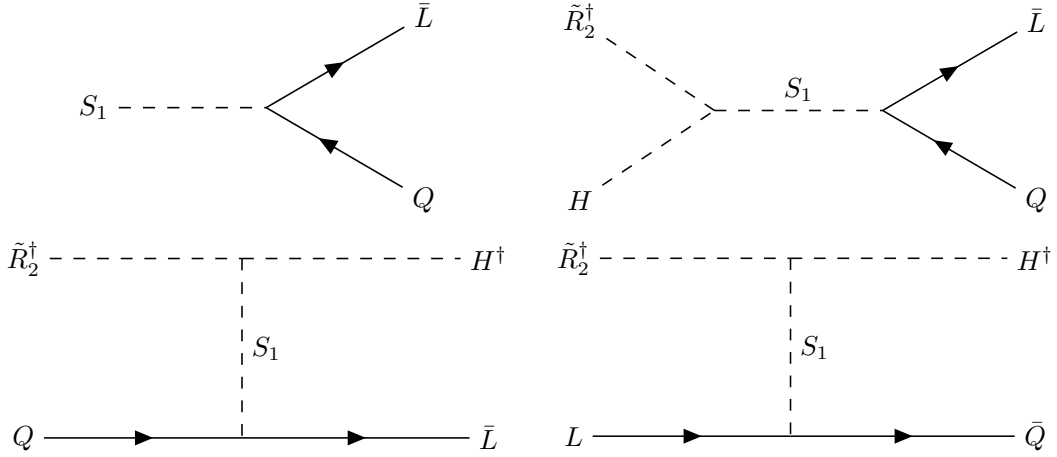


Figure 3: Top left: Decay diagram for $S_1 \rightarrow \bar{L}\bar{Q}$. Top right and bottom row: Scattering diagrams involved in the $\Delta L = 2$ washout.

decays (see Fig. 3 top left). Since the total widths of S_1 and S_1^* must remain equal for CPT to be conserved, we require that this latter source of CP -violation is equal in magnitude but opposite in sign compared to the former. Note that, in this model, there are no 1-loop diagrams with vertex corrections. Note further that 1-loop self-energy diagrams with scalar fields in the loop do not contribute to CP -violation, since the corresponding interference term is purely real. The amount of CP -violation ϵ is defined as

$$\epsilon \equiv \text{BR}(S_1 \rightarrow H\tilde{R}_2^\dagger) - \text{BR}(S_1^* \rightarrow H^\dagger\tilde{R}_2), \quad (3.1)$$

which for the model described in Sec. 2 and using the diagrams shown in Fig. 2 is given by (c.f. Refs. [48–50])

$$\epsilon = \frac{2}{\pi} \frac{|v_{B-L}|^2 \text{Im}[\lambda_1 \lambda_3^* \text{Tr}(g_3^\dagger g_1)]}{4 \text{Tr}(g_1^\dagger g_1) m_{S_1}^2 + |\lambda_1 v_{B-L}|^2} \frac{x}{1-x}, \quad (3.2)$$

where $x \equiv m_{S_1}^2/m_{S_3}^2$.

In addition to the decays of S_1 , the present model will also lead to $\Delta L = 2$ washout processes (see Fig. 3 top right and bottom row), as well as both $\Delta L = 2$ and $\Delta L = 0$ processes with external S_1 legs. Since we neglect thermal effects we also treat all light fields as massless, including \tilde{R}_2 and all SM fields. In this limit the two-to-two scattering processes with external S_1 legs are IR divergent, and we therefore neglect them. This is further motivated since we expect that the main source of washout comes from the S_1 -mediated $\Delta L = 2$ processes (without external S_1 legs) because they are not suppressed by the small S_1 number density during the regime of strong washout. In Sec. 5 we test the validity of this statement by artificially modifying the corresponding set of equations.

By including the processes shown in Figs. 2 and 3 while taking $\tilde{R}_2^\dagger \leftrightarrow L + \bar{d}$ to be in chemical equilibrium we arrive at the following set of Boltzmann equations (c.f. Ap-

pendix A),

$$zHn_\gamma \frac{d\eta_{S_1^+}}{dz} = -\gamma_D \left[\frac{\eta_{S_1^+}}{\eta_{S_1}^{\text{eq}}} - 1 + \epsilon c_+ \frac{\eta_{\Delta(B-L)}}{\eta_{B-L}^{\text{eq}}} \right], \quad (3.3)$$

$$zHn_\gamma \frac{d\eta_{S_1^-}}{dz} = -\gamma_D \left[\frac{\eta_{S_1^-}}{\eta_{S_1}^{\text{eq}}} - c_- \frac{\eta_{\Delta(B-L)}}{\eta_{B-L}^{\text{eq}}} \right], \quad (3.4)$$

$$\frac{zHn_\gamma}{c_{\Delta(B-L)}} \frac{d\eta_{\Delta(B-L)}}{dz} = \frac{\gamma_D}{2} \left[r \frac{\eta_{S_1^-}}{\eta_{S_1}^{\text{eq}}} + \epsilon \left(\frac{\eta_{S_1^+}}{\eta_{S_1}^{\text{eq}}} - 1 \right) \right] - \left(c_- r \frac{\gamma_D}{2} + c_+ \gamma_W \right) \frac{\eta_{\Delta(B-L)}}{\eta_{B-L}^{\text{eq}}}. \quad (3.5)$$

Here $z \equiv m_{S_1}/T$ is a time-evolution variable, where T is the temperature, H is the Hubble rate, n_γ is the photon number density, and $\eta_X = n_X/n_\gamma$ is the number density of particle X normalized to the photon number density, where a superscript *eq* denotes the equilibrium density and where $\eta_{\Delta(B-L)}$ denotes the net $B-L$ number density. Furthermore, γ_D and γ_W are the equilibrium reaction rate densities for the decay of S_1 and washout, respectively. Furthermore, r is given by

$$r \equiv \text{BR}(S_1 \rightarrow H\tilde{R}_2^\dagger) + \text{BR}(S_1^* \rightarrow H^\dagger\tilde{R}_2), \quad (3.6)$$

while c_\pm and $c_{\Delta(B-L)}$ are $\mathcal{O}(\text{few})$ numerical coefficients that depend on the number of thermally active fermion species. See Appendix A for a derivation of Eqs. (3.3) – (3.5) as well as definitions of the different variables. Lastly, rather than tracking the evolution of S_1 and S_1^* we find it more convenient to use S_1^\pm where

$$\eta_{S_1^+} \equiv \frac{1}{2}(\eta_{S_1} + \eta_{S_1^*}), \quad (3.7)$$

$$\eta_{S_1^-} \equiv \frac{1}{2}(\eta_{S_1} - \eta_{S_1^*}). \quad (3.8)$$

Note that in the equation for $\eta_{S_1^-}$ the corresponding equilibrium is reached when its density vanishes, $\eta_{S_1^-}^{\text{eq}} = 0$, while $\eta_{S_1^+}$ reaches equilibrium when the densities for S_1 and S_1^* are equal, such that $\eta_{S_1^+}^{\text{eq}} = \eta_{S_1^*}^{\text{eq}}$. The first terms in both Eqs. (3.3) and (3.4) therefore have the form

$$zHn_\gamma \frac{d\eta_{S_1^\pm}}{dz} \supset -\gamma_D \frac{1}{\eta_{S_1}^{\text{eq}}} \left(\eta_{S_1^\pm} - \eta_{S_1^\pm}^{\text{eq}} \right). \quad (3.9)$$

The same form appears in the first two terms of Eq. (3.5) although with additional factors ϵ and r . Since S_1 is charged under $SU(3)_c$, it can be produced in $gg \rightarrow S_1 S_1^*$ where g is a gluon. We expect the rate of this reaction to be rapid in the very early Universe, at $T \gg m_{S_1}$, but quickly fall off around $T \sim m_{S_1}$ due to its dependence on the square of the S_1 abundance (in the limit of $\eta_{S_1^-} \rightarrow 0$). To account for this interaction we set the initial S_1^+ and S_1^- abundances at $z \ll 1$ to their equilibrium values when we numerically solve the Boltzmann equations in Sec. 5.

We note that in Eqs. (3.3) – (3.5) there is no dependence on the mass of \tilde{R}_2 . Since we assume a large hierarchy $m_{S_1} \gg m_{\tilde{R}_2}$, we treat \tilde{R}_2 as ultra-relativistic during the generation

of the asymmetry, i.e. at temperatures $0.01 \lesssim z \lesssim 100$, and its mass therefore does not enter the equations. Furthermore, in the limit of this hierarchy, the washout diagrams in Fig. 3 (top right and bottom row) are roughly proportional to the neutrino mass, i.e. they have the same dependence on the mass and two couplings of S_1 as m_ν does. What separates them is that m_ν depends on the Higgs VEV as well as the coupling g_2 between \tilde{R}_2 and the SM, whereas the washout diagrams do not.

In our model the asymmetry is generated by $\Delta L = 2$, $\Delta B = 0$ interactions, and it would therefore have been enough to track the L asymmetry rather than $B - L$ asymmetry in Eq. (3.3), since all the B violation cancels out. We have chosen to track the $B - L$ asymmetry for generality. However, note that the observed BAU is completely contained in the baryon sector, and to compare our results with observations we use the conversion [51]

$$Y_{\Delta B} = \frac{79}{51} Y_{\Delta(B-L)}. \quad (3.10)$$

An additional factor $d_{\text{rec}} \approx 1/29$ should also be included to account for the change in entropy density between the early and late Universe. Note that this factor is slightly smaller than in the standard type-I seesaw leptogenesis since we have included the relativistic degrees of freedom of \tilde{R}_2 . Furthermore, while a relativistic \tilde{R}_2 can lead to the reaction $\tilde{R}_2^\dagger \leftrightarrow L + \bar{d}$ being in chemical equilibrium, this does not modify the sphaleron conversion factor, since the sphaleron only involves the SM fermions. This reaction does however modify the overall chemical equilibrium relations between different particle species, c.f. Appendix A.

As mentioned in Sec. 2, the leptokuark model considered here could be extended with right-handed neutrinos N that couple to S_1 and \bar{d}^c at tree-level. For Majorana N this could lead to additional channels of CP -violation in S_1 decays via vertex corrections, and therefore a possible enhancement of the asymmetry [30–32]. However, if N is lighter than S_1 it could potentially lead to additional N -mediated $\Delta L = 2$ washout channels that erase the asymmetry, depending on its mass and the size of its coupling to the SM. If N does not have a Majorana mass, it could still affect the leptogenesis mechanism as an external state by leading to additional S_1 -mediated $\Delta L = 2$ washout channels.

4 Phenomenology

The model presented in Sec. 2 is subject to a number of experimental constraints, as has been discussed in recent works [24, 25]. Note that each such experimental observable will either depend on the mass of \tilde{R}_2 or rely on couplings that are not present in the leptogenesis mechanism or neutrino mass generation. In the limit of large hierarchy $m_{S_1} \gg m_{\tilde{R}_2}$, both the neutrino mass and final baryon asymmetry are independent of $m_{\tilde{R}_2}$, as discussed in Secs. 2 and 3, respectively. We can therefore always tune $m_{\tilde{R}_2}$ in such a way that the model is unconstrained in the region of successful leptogenesis and neutrino mass generation, so long as such a region exists while still respecting the hierarchy $m_{S_1} \gg m_{\tilde{R}_2}$, which will be the case for each observable below. The model is subject to different constraints, depending most significantly on $m_{\tilde{R}_2}$, and could lead to observable signatures in each phenomenological probe discussed below, but is not required to do so in order for the leptogenesis mechanism

to work. For this reason, we comment on various relevant observables in this section but do not attempt to show exclusion lines.

4.1 Colliders

Leptoquarks could be produced in collider experiments such as the LHC [52–63]. For the model we consider here, only \tilde{R}_2 could potentially be within the reach of collider searches, since we take the masses of S_1 and S_3 to be much greater. The most stringent constraint $m_{LQ} > 1460$ GeV for $g_2^{33} = 3$ at 95% C.L. comes from a search by ATLAS for pair production of scalar leptoquarks decaying into b and τ [64]. More stringent constraints could be set in future colliders such as FCC-ee [65].

4.2 Neutrinoless double beta decay

Neutrinoless double beta ($0\nu\beta\beta$) decay is the most sensitive low-scale experimental probe of lepton number violation in the first-generation fermions [66–68]. The model from Sec. 2 can lead to $0\nu\beta\beta$ decay via the SMEFT operators from Eq. (2.3) [24, 25, 38–40, 69–71]. From Ref. [40] we have the constraints

$$(C_{\tilde{d}LQLH1}^{1111})^{-1/3} < 2.4 \times 10^5 \text{ GeV}, \quad (C_{\tilde{d}LQLH2}^{1111})^{-1/3} < 1.4 \times 10^5 \text{ GeV}, \quad (4.1)$$

which are based on results from the KamLAND-Zen experiment at 90% C.L. [72]. Using the relations in Eq. (2.4) while keeping all couplings equal to one, choosing $v_{B-L} = m_{S_1}$, and keeping $m_{\tilde{R}_1} = 5$ TeV, we find the constraint $m_{S_1} > 5.7 \times 10^8$ GeV. Instead choosing $g_1^{11} = 0.025$, $v_{B-L} = 3m_{S_1}$, and $\lambda_1 = 10^{-3}$ following benchmark point BM1 in Sec. 5, we have $m_{S_1} > 4.3 \times 10^4$ GeV.

4.3 Rare kaon decays

Rare kaon decays $K \rightarrow \pi\nu\nu$ are the second most sensitive probe of lepton number violation induced by dimension-7 SMEFT operators [23, 40, 73–75], and the most sensitive overall beyond the first generation fermions. The operator $\mathcal{O}_{\tilde{d}LQLH1}^{prst}$ from Eq. (2.3) can lead to such lepton-number-violating rare kaon decays. Currently the most stringent constraint $(C_{\tilde{d}LQLH1}^{2r1t})^{-1/3} < 2.2 \times 10^4$ GeV [40] comes from the charged mode $K^+ \rightarrow \pi^+\nu\nu$ at the NA62 experiment at 90% C.L. [76, 77]. For BM1 with $g_1^{1t} = 0.025$ we find $m_{S_1} > 32$ GeV. These constraints are based on searches for the SM mode $K^+ \rightarrow \pi^+\nu\bar{\nu}$, while a dedicated search for the $\Delta L = 2$ mode could be possible in future experiments [78]. The future KOTO-II experiment [79] will put even more stringent constraints on the corresponding neutral mode $K_L \rightarrow \pi^0\nu\nu$.

The corresponding rare B -meson decay $B \rightarrow K\pi\nu\bar{\nu}$ can also potentially lead to signals of lepton number violation. However, existing constraints on the scale of NP from this decay are less stringent than those coming from kaon decays, in the case where NP couples to all quark flavours equally [40]. For flavour non-universal NP that dominantly couples to the third generation, B decays could potentially provide the most stringent constraints. A recent measurement at Belle II [80] shows an excess of events which could be due to

NP [81], but would lead to a significant over-production of the neutrino mass in the case of lepton number violation [75].

4.4 Baryon number violation

In Tab. 1 the leptoquarks S_1 , \tilde{R}_2 , and S_3 are denoted as carrying a non-zero baryon number as well as lepton number. With this assignment, baryon number is conserved in all couplings in the corresponding Lagrangian in Eq. (2.1). However, as mentioned above, S_1 and S_3 can have diquark couplings as well as leptoquark couplings, i.e. they can potentially interact with a pair of quarks at tree-level. This would violate both lepton- and baryon number, $\Delta B = -\Delta L = 1$. If present, such couplings could potentially lead to rapid proton decay at tree-level [30–32, 82, 83]. We can predict the rate of proton decay in our model, e.g. via the mode $p \rightarrow \pi^0 e^+$, using the nucleon form factor [84]

$$\langle \pi | \epsilon_{abc} \left(q^a C P_{\Gamma} q^b \right) P_{\Gamma'} q^c | \psi \rangle = P_{\Gamma'} \left[W_0^{\Gamma\Gamma'}(\mu, p^2) - \frac{i \not{p}}{m_{\psi}} W_1^{\Gamma\Gamma'}(\mu, p^2) \right] u_{\psi}, \quad (4.2)$$

where $W_0^{\Gamma\Gamma'}$ and $W_1^{\Gamma\Gamma'}$ are the form factors, μ is the characteristic energy scale, p is the momentum exchange, $u_{\psi} \in \{n, p\}$ and $q \in \{u, d\}$ are nucleon- and quark spinors, respectively, C is the charge conjugation operator, P_{Γ} is a projection operator for chiral indices $\Gamma, \Gamma' \in \{L, R\}$, and a, b, c are color indices. Considering the coupling of S_1 to doublet quarks such that $\mathcal{L} \supset -g_1^{ij} \bar{Q}_i i \sigma_2 Q_j^c S_1 + \text{h.c.}$ we have the corresponding matrix element

$$\mathcal{M}_{p \rightarrow \pi^0 e^+} = \langle \pi^0 e^+ | C_{Q^3 L}^{1111}(\mu_{\text{NP}}) \mathcal{O}_{Q^3 L}^{1111} | p \rangle, \quad (4.3)$$

for the operator

$$\mathcal{O}_{Q^3 L}^{prst} = \epsilon_{abc} \epsilon_{ij} \epsilon_{mn} (\bar{Q}_p^{c ai} Q_r^{bj}) (\bar{Q}_s^{cm} L_t^n) \quad (4.4)$$

and Wilson coefficient

$$C_{Q^3 L}^{prst} = \frac{g_1^{pr} g_1^{st}}{m_{S_1}^2}. \quad (4.5)$$

Here we have neglected the contribution from S_3 since we expect S_1 to dominate. We then have

$$\mathcal{M}_{p \rightarrow \pi^0 e^+} = U'(\mu_{\text{NP}}, \mu_0) C_{Q^3 L}(\mu_{\text{NP}}) \left[W_0^{LL}(\mu_0, m_e^2) - \frac{i \not{p}}{m_{\psi}} W_1^{LL}(\mu_0, m_e^2) \right] u_p P_L \bar{u}_e, \quad (4.6)$$

where μ_0 is the energy scale of the decay, $\mu_{\text{NP}} \sim m_{S_1}$ is the scale of New Physics, and

$$U'(\mu_{\text{NP}}, \mu_0) = U_i^{N_f=6}(\mu_{\text{NP}}, m_t) U_i^{N_f=5}(m_t, m_b) U_i^{N_f=4}(m_b, \mu_0) \quad (4.7)$$

accounts for the running of the strong coupling constant α_S , where [85]

$$U_i^{N_f}(\mu_1, \mu_2) = \left(\frac{\alpha_S(\mu_2)}{\alpha_S(\mu_1)} \right)^{\gamma_i^0/2\beta_0} \left[1 + \left(\frac{\gamma_1}{2\beta_0} - \frac{\beta_1 \gamma_0}{2\beta_0^2} \right) \frac{\alpha_S(\mu_2) - \alpha_S(\mu_1)}{4\pi} \right], \quad (4.8)$$

for the coefficients

$$\beta_0 = 11 - \frac{2}{3}N_f, \quad \beta_1 = 102 - \frac{38}{3}N_f, \quad (4.9)$$

$$\gamma_0 = -4, \quad \gamma_1 = -\left(\frac{14}{3} + \frac{4}{9}N_f\right), \quad (4.10)$$

where N_f is the number of fermions that carry colour charge.

Currently the most stringent constraints on the $p \rightarrow \pi^0 e^+$ lifetime is $\tau_{p \rightarrow \pi^0 e^+} > 1.6 \times 10^{34}$ years at 90% C.L. coming from the Super-Kamiokande experiment [86]. Using the form factors given in Ref. [84] we find $C_{Q^3 L}^{1111} \lesssim (2.1 \times 10^{13} \text{ GeV})^{-2}$. Choosing the parameters $m_{S_1} = 10^8 \text{ GeV}$ and $g_1^{11} = 0.025$ following benchmark point BM1 in Sec. 5 we then find that we require $g_1'^{11} \lesssim 0.9 \times 10^{-9}$ in order to satisfy the experimental bound on proton decay. This is a very small coupling, however there are several caveats which should be considered at this point. Firstly, the neutrino mass generation mechanism depends chiefly on the couplings to the third generation down-type quark, while for this proton decay mode only the first generation couplings are relevant at tree-level. Due to loop suppression and the smallness of the V_{td} and V_{ub} CKM matrix elements, loop-level proton decays that utilize the quark couplings to third generation quarks have a negligible decay width. In a scenario where leptoquarks couple mainly to the third generation, the proton decay constraint could therefore more easily be satisfied. Secondly, if one only considers leptogenesis without requiring that the model also leads to the observed neutrino mass, it is possible to have much higher masses for S_1 and S_3 (c.f. Sec. 5), which would significantly increase the proton lifetime. This would underproduce the neutrino mass, and a different mechanism would then be required for its successful generation (e.g. type-I seesaw). Lastly there could be cancellations between different contributions to the decay width of the proton coming from e.g. S_3 or other components of a more complete model.

Note that with g_1' we could also have the proton decay modes $p \rightarrow \pi^+ \nu$ mediated by a dimension-7 operator involving \tilde{R}_2 - S_1 mixing. This mode has a less stringent bound compared to that of $p \rightarrow \pi^0 e^+$, namely $\tau_{p \rightarrow \pi^+ \nu} > 3.9 \times 10^{32}$ years at 90% C.L. again from the Super-Kamiokande experiment [87]. The corresponding decay rate will depend on $m_{\tilde{R}_2}$ in addition to g_1' , making it two parameters that are not involved in the leptogenesis or neutrino mass generation mechanisms in the $m_{S_1} \gg m_{\tilde{R}_2}$ limit.

As mentioned in Secs. 2 and 3, the leptoquark model could be extended with right-handed neutrinos N . If N has a sizable Majorana mass, its coupling to S_1 and \bar{d}^c could lead to potentially observable neutron-antineutron (n - \bar{n}) oscillation [88–90]. For this mechanism to work, S_1 additionally needs diquark couplings to a pair of quark doublets or up- and down-type singlets, same as for proton decay. The corresponding n - \bar{n} oscillation diagram then consists of two S_1 mediators and one N mediator with six external quark legs.

4.5 Flavour violation

For flavour off-diagonal couplings there are several observables of flavour physics that could constrain the leptoquark model [24, 25], e.g. charged lepton-flavour-violating processes such as $\mu \rightarrow e\gamma$, $\mu N \rightarrow eN$ (where N is a nucleus), $K_L \rightarrow \mu^\pm e^\mp$, and $K^+ \rightarrow \pi^+ \mu^+ e^-$, or

deviations from the SM in quark-flavour observables such as $K \rightarrow \pi \nu \bar{\nu}$. Note that this latter observable is distinct from the lepton-number-violating process $K \rightarrow \pi \nu \nu$ discussed in Sec. 4.3. In our present scenario the leptoquark \tilde{R}_2 is the field that is potentially susceptible to such constraints since it is the lightest.

From Refs. [24] and [25] we find that the most stringent such constraint comes from $\mu N \rightarrow e N$ conversion using gold at the SINDRUM II experiment, namely $\text{BR}(\mu N \rightarrow e N)_{\text{Au}} < 7 \times 10^{-13}$ at 90% C. L. [91], where BR here denotes the rate of conversion normalized to the muon capture rate. We then have the constraint $g_2^{11} g_2^{21} / m_{\tilde{R}_2}^2 < (500 \text{ TeV})^2$ [24].

For a completely general flavour structure we see that constraints coming from flavour violation are more stringent than those coming from collider searches (c.f. Sec. 4.1). However, note that neutrino mass generation most dominantly depends on the third generation couplings, for which the flavour constraints are not applicable. In Sec. 5 we therefore choose to evaluate benchmark points with \tilde{R}_2 close to collider constraints, and neglect the constraints coming from flavour physics.

5 Results

To find the model parameters that lead to the successful generation of a BAU and neutrino masses that both match observations, we numerically solve the Boltzmann equations from Eqs. (3.3) – (3.5) and overlap these results with the neutrino mass from Eq. (2.5). We define a benchmark point BM1 as

BM1: $m_{S_1} = 10^8 \text{ GeV}, m_{\tilde{R}_2} = 5 \text{ TeV}, m_{S_3} = 3m_{S_1}, v_{B-L} = 3m_{S_1},$ $g_1 = 0.025, g_2 = 1, g_3 = g_1, \lambda_1 = 10^{-3}, \lambda_3 = i\lambda_1$

leading roughly to the observed neutrino mass. Note that we take λ_3 to be purely imaginary. We keep these relations between the parameters related to S_1 and S_3 in order for our approximations to always be valid, i.e. that we can neglect the dynamics of S_3 etc., such that below when we vary e.g. g_1 we also vary g_3 . We consider only third generation couplings $g_i^{mn} \propto \delta_{m3} \delta_{n3}$ for $i \in \{1, 2, 3\}$ since these are the couplings most relevant for neutrino mass generation. We do not attempt to exactly reproduce the observed neutrino mass spectrum, only its characteristic scale. We furthermore assume that there are three thermally active fermion generations such that $N = 3$ (c.f. Appendix A), in order to be consistent in the low- m_{S_1} parameter space regions. We find that varying N generally has an $\mathcal{O}(1)$ effect on the results.

In Fig. 4 we show regions in the g_1 - m_{S_1} plane that lead to the observed value for η_B (green) and m_ν (orange), for the parameters defined as BM1 but varying g_1 , m_{S_1} , and λ_1 . The lower edge of the m_ν band corresponds to $m_1 = 0$, while the upper edge corresponds to the maximum value of $m_1 < 0.30 \text{ eV}$ (c.f. Sec. 2). We see that there are regions of parameter space in which these regions overlap, such that the model simultaneously leads to both the observed neutrino mass scale as well as the observed BAU. Note that the green region appears as a line that carves out an area towards the right. Within this region (to the right) the generated asymmetry is larger than that which is observed, and outside it is smaller. For smaller couplings λ_1 this region grows, since the washout coming from

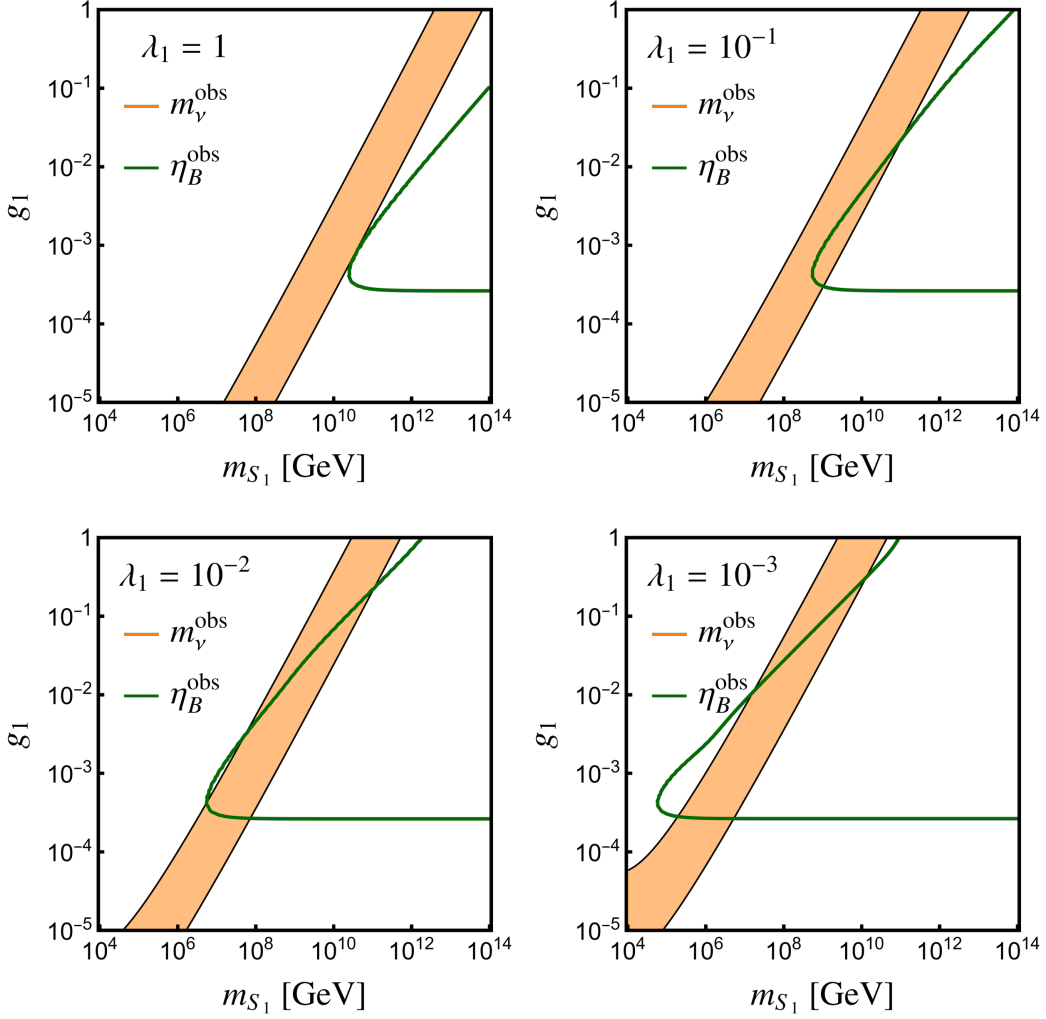


Figure 4: Contour plots in the g_1 - m_{S_1} plane showing the regions in which the observed value for η_B (green) and m_ν (orange) is produced, for different values of the coupling λ_1 and indicated in the top-left corner of each plot. Other parameters are chosen according to benchmark point BM1 (see text).

$\Delta L = 2$ scatterings is decreased. However, if λ_1 is decreased to smaller values than the ones shown in Fig. 4, e.g. for $\lambda_1 \lesssim 10^{-4}$, the green line disappears completely. The reason for this is that for small λ_1 the CP -violation also decreases with λ_1 , such that for small enough couplings the observed BAU can no longer be generated. Similar effects can be seen in the variation of g_1 , for small enough values η_B becomes smaller than η_B^{obs} , independently of the value of λ_1 . Whichever of g_1 and λ_1 is smaller is the one that governs the size of the CP -violating parameter ϵ , as can be seen from the expression in Eq. (3.2). For large enough couplings g_1 or λ_1 the value of η_B is again too small, due to increased $\Delta L = 2$ washout, as can be seen in the top-left part of each plot. Note that the η_B^{obs} -line in this region is almost parallel to that of m_ν^{obs} . The reason for this is that the $\Delta L = 2$ washout processes and m_ν both have the same proportionality to m_{S_1} , g_1 , and λ_1 in the limit of large

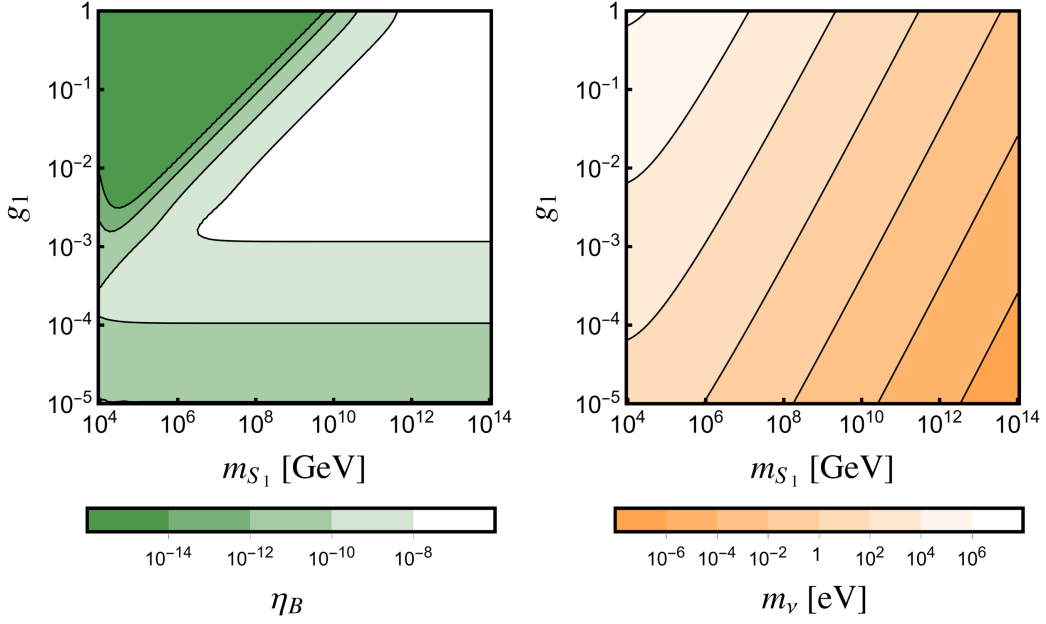


Figure 5: Contour plots in the g_1 - m_{S_1} plane showing the value of η_B (left) and m_ν (right). Other parameters are chosen according to benchmark point BM1 (see text).

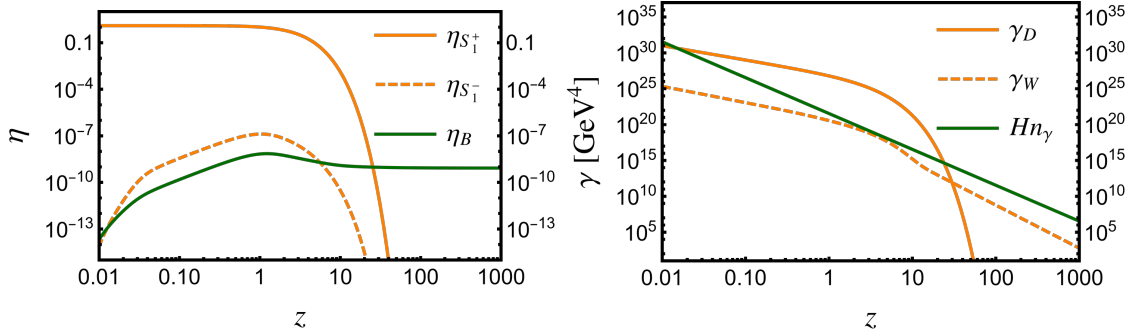


Figure 6: Evolution of $\eta_{S_1^+}$, $\eta_{S_1^-}$, and η_B with respect to $z \equiv m_{S_1}/T$ (left), as well as the Hubble rate H multiplied by the photon number density n_γ and corresponding reaction rate densities γ_D and γ_W (right), for the parameters described as benchmark point BM1 in the text.

hierarchy, $m_{S_1} \gg m_{\tilde{R}_2}$. Having a large neutrino mass will therefore also lead to having a large washout.

In Fig. 5 we show the values of η_B (left) and m_ν (right) for the parameters defined as BM1 but while varying g_1 and m_{S_1} . We see that η_B decreases proportionally to the square of g_1 for small values of g_1 , as expected from Eq. (3.2). In contrast, the decrease in η_B with increasing g_1 in the large-washout regime (top left) is comparatively rapid. In Fig. 5 (left) we do not resolve values of η_B smaller than 10^{-15} .

In Fig. 6 (left) we show the time-evolution of $\eta_{S_1^+}$, $\eta_{S_1^-}$, and η_B (c.f. Sec. 3) with respect to $z \equiv m_{S_1}/T$ for the set of parameters defined as BM1. We see that the S_1^+ abundance

starts falling off around $z \sim 1$ and vanishes well before $z = 100$. The S_1^- abundance increases as η_B grows but similarly falls off for $z \gtrsim 1$. The baryon asymmetry η_B initially grows as S_1 decays, then gets slightly reduced around $1 \lesssim z \lesssim 10$ due to the $\Delta L = 2$ washouts, after which it freezes out. Note that we here show the value of η_B after having applied the sphaleron conversion factor and dilution factor d_{rec} (c.f. Sec. 3), rather than showing the $B - L$ asymmetry $\eta_{\Delta B-L}$, in order for easier comparison with the observed value $\eta_B^{\text{obs}} \approx 6.20 \times 10^{-10}$. In Fig. 6 (right) we show the corresponding reaction rate densities γ_D and γ_W , as well as the Hubble rate H multiplied by the photon number density n_γ . When the rates are greater than Hn_γ they significantly affect the relevant particle number densities, and while they are smaller they do not have a large effect. Comparing with Fig. 6 (left) we see that S_1^+ decays are significant while γ_D is large, which is the era when η_B is generated. Around $1 \lesssim z \lesssim 10$ the washout rate approaches Hn_γ , which leads to a small dip in η_B . If the washout rate were to overtake the expansion, the asymmetry would be significantly reduced, if not removed completely.

In Sec. 3 we neglected the effects of $\Delta L = 0$ and $\Delta L = 2$ two-to-two processes with external S_1 legs. The $\Delta L = 0$ processes can have the effect of reducing the S_1 abundance during the temperature regime in which the out-of-equilibrium decays occur, and the $\Delta L = 2$ processes lead to additional washout channels. We can estimate the effects of such processes by including artificial terms proportional to $\gamma_D(\gamma_W/\gamma_D)|_{z=1}(\eta_{S_1^+}/\eta_{S_1^+}^{\text{eq}})$ in the first Boltzmann equation, Eq. (3.3), to account for the S_1 depletion, and the same but with an additional factor $\eta_{\Delta(B-L)}/\eta_{B-L}^{\text{eq}}$ in the third Boltzmann equation, Eq. (3.5), to account for the additional washout channels. Here the factor $\gamma_D(\gamma_W/\gamma_D)|_{z=1}$ is included since we expect the processes to have a similar magnitude to that of γ_W but a thermal profile similar to that of γ_D . Doing this we find at most an $\sim \mathcal{O}(1)$ reduction of the final asymmetry for the relevant parameter space.

In Figs. 4 and 5 the \tilde{R}_2 mass was chosen as $m_{\tilde{R}_2} = 5$ TeV, while the m_{S_1} -axis goes down to 10^4 GeV. Towards this edge the validity of the approximation $m_{S_1} \gg m_{\tilde{R}_2}$ starts becoming unfounded. The neutrino mass calculation takes $m_{\tilde{R}_2}$ into account, but for η_B we assumed it to vanish, $m_{\tilde{R}_2} \rightarrow 0$. We suspect that having non-zero $m_{\tilde{R}_2} \lesssim m_{S_1}$ would increase the value of η_B in the limit $m_{\tilde{R}_2} \rightarrow m_{S_1}$ since the $\Delta L = 2$ washouts become thermally suppressed, so long as the phase space suppression in S_1 decays is not too large.

Furthermore, while m_ν is independent of $m_{\tilde{R}_2}$ in the limit $m_{S_1} \gg m_{\tilde{R}_2}$, we note that part of the successful parameter space in Fig. 4 lies in regions where m_{S_1} is only one or a few orders of magnitude greater than $m_{\tilde{R}_2}$, for which m_ν is somewhat dependent on $m_{\tilde{R}_2}$, such that increasing $m_{\tilde{R}_2}$ would move the orange band towards the top-left corner in each plot. Taking $m_{\tilde{R}_2} = 500$ TeV to agree with the first- and second generation coupling constraints from flavour physics (c.f. Sec. 4.5) we find that we have an overlap of m_ν^{obs} and η_B^{obs} only for smaller values of λ_1 .

In this analysis we have not reproduced the neutrino mass spectrum, only its characteristic scale. The full spectrum can be accommodated by using experimental values for the mass splittings Δm_{12}^2 and Δm_{13}^2 (in normal hierarchy) and solving Eq. (2.5) for g_1 and g_2 for an unknown lightest neutrino mass m_1 . Between the minimum value $m_1 = 0$ and highest allowed value $m_1 \approx 0.30$ eV (c.f. Sec. 2) the shape of the diagonalized neutrino mass matrix

\hat{m}_ν varies greatly. For $m_1 = 0$ the neutrino mass matrix \hat{m}_ν only has non-zero entries in the $(m_1)_{22}$ and $(m_1)_{33}$ components, where the latter is almost an order of magnitude greater than the former. For the maximum value of m_1 however, \hat{m} is close to being proportional to the unit matrix. In this case the hierarchy of leptoquark couplings to the SM fermions will need to be inverted compared to that of the SM Yukawa couplings, in order for one to compensate for the other (c.f. Eq. (2.5)). This is in conflict with the benchmark point used for the leptogenesis mechanism in this section, however note that, neglecting spectator effects, the leptogenesis mechanism we consider here is essentially flavour-blind, such that the same results would apply for $g_2^{(11)}$ as $g_2^{(33)}$.

6 Conclusion

We have shown that the leptoquark model described in Sec. 2 can lead to both neutrino mass generation and leptogenesis while avoiding existing experimental constraints. For a small enough mass of \tilde{R}_2 and large enough couplings to the SM, the model can potentially be within the reach of future experiments such as e.g. $0\nu\nu\beta$ decay searches or at colliders. Note however that the leptogenesis mechanism, and to some extent also neutrino mass generation, are decoupled from the mass of \tilde{R}_2 .

The leptoquark model was essentially chosen as an example, following these results we may expect a similar situation to appear in other radiative neutrino mass models, or in the inverted hierarchy $m_{\tilde{R}_2} \gg m_{S_1}$, i.e. it is probably possible to have both neutrino masses and leptogenesis in a wide range of scenarios, such as the different UV-completions of 4-fermion $\Delta L = 2$ dimension-7 SMEFT operators [92–100]. The reason we may expect this is that the detailed properties of the new particles, such as Lorentz structure, representation under the SM gauge group, and number of possible tree-level interactions with the SM, generally enter as $\mathcal{O}(\text{few})$ factors in the reaction rates involved in the Boltzmann equations, as well as in the neutrino mass generation mechanism, while the topologies remain the same or very similar. For models where an up-type quark participates in the radiative neutrino mass diagram there may be an even greater successful parameter space available due to the large mass of the top quark. However, these are speculations, and a full study would be warranted to confirm whether such statements are true.

We found that the S_1 -mediated $\Delta L = 2$ washout processes are proportional to the neutrino mass, such that a large neutrino mass would also produce a large washout, leading to the erasure of any generated baryon asymmetry. The smallness of the neutrino mass could then potentially be explained from anthropic arguments (see e.g. Ref. [101]).

We have neglected thermal effects in the leptogenesis mechanism. This led us to drop some sub-leading washout diagrams which a quick estimate showed could have small but non-vanishing effect, c.f. Sec. 5. We have furthermore neglected corrections from bound state formation [102], which can be important for particles charged under a strongly coupled gauge group such as $SU(3)_c$ of the SM. However, bound state formation is unlikely to be significant in the low- z regions during which the BAU is generated in most of our successful parameter space.

Acknowledgements

I would like to thank Motoi Endo, Chandan Hati, and Peter Maták for helpful discussions. I acknowledge support from the Japan Society for the Promotion of Science (JSPS) Grant-in-Aid for Scientific Research B (No. 21H01086 and 23K20847).

A Boltzmann equations

In this Appendix we give a detailed derivation of the Boltzmann equations from Sec. 3 following Refs. [47, 50]. The time-evolution of a particle's number density can be written as

$$zHn_\gamma \frac{d\eta_X}{dz} = - \sum_{i,j,\dots} [X \cdots \leftrightarrow ij \cdots]. \quad (\text{A.1})$$

Here X denotes the particle species, $z \equiv m_X/T$ is the time variable, where m_X is the mass of X and T is the temperature, and $\eta_X = n_X/n_\gamma$ is the number density of X normalized to the photon number density n_γ given by

$$n_\gamma = \frac{2\zeta(3)}{\pi^2} T^3, \quad (\text{A.2})$$

where $\zeta(3) \approx 1.20$ is the Riemann zeta function. Furthermore, H is the Hubble rate given by

$$H = \frac{1.66\sqrt{g_*}}{m_{\text{Pl}}} T^2 \quad (\text{A.3})$$

where $m_{\text{Pl}} \approx 1.2 \times 10^{19}$ GeV is the Planck mass and g^* is the number of relativistic degrees of freedom, where in the early Universe our model leads to $g^* = 112.75$, which is greater than in the SM due to the presence of a relativistic \tilde{R}_2 . Note that we have here ignored the effects of a relativistic \tilde{R}_2 which could add six degrees of freedom. The square brackets on the RHS of Eq. (A.1) are given by

$$[X \cdots \leftrightarrow ij \cdots] = \frac{\eta_X \cdots}{\eta_X^{\text{eq}} \cdots} \gamma^{\text{eq}}(X \cdots \rightarrow ij \cdots) - \frac{\eta_i \eta_j \cdots}{\eta_i^{\text{eq}} \eta_j^{\text{eq}} \cdots} \gamma^{\text{eq}}(ij \cdots \rightarrow X \cdots). \quad (\text{A.4})$$

Here i and j are additional particles that X interact with, and the dots denote that more particle species can be included in both the initial and final states. The summation in Eq. A.1 goes over all such interactions that involve X . Furthermore, η_X^{eq} is the normalized equilibrium number density of X given by

$$\eta_X^{\text{eq}} = \frac{g_X}{4\zeta(3)} z^2 K_2(z), \quad (\text{A.5})$$

where g_X is the number of degrees of freedom of X and $K_\nu(z)$ is the modified Bessel function of the second kind. Note that the equilibrium number densities of a given particle and its corresponding antiparticle are equal. The equilibrium reaction rate density γ^{eq} for a two

body decay $X \rightarrow ij$ is given by

$$\gamma^{\text{eq}}(X \rightarrow ij) = \eta_X^{\text{eq}} n_\gamma \frac{K_1(z)}{K_2(z)} \Gamma(X \rightarrow ij), \quad (\text{A.6})$$

where

$$\Gamma(X \rightarrow ij) = \frac{1}{1 + \delta_{ij}} \frac{m_X^2 - m_i^2 - m_j^2}{16\pi m_X^3} |\mathcal{M}(X \rightarrow ij)|^2 \quad (\text{A.7})$$

is the decay width for a corresponding matrix element $\mathcal{M}(X \rightarrow ij)$. For a two-to-two scattering $Xa \rightarrow ij$ the equilibrium reaction rate density is given by

$$\gamma^{\text{eq}}(Xa \rightarrow ij) = \frac{T}{64\pi^4} \int_{s_{\min}}^{\infty} ds \sqrt{s} \hat{\sigma}(Xa \rightarrow ij) K_1\left(\frac{\sqrt{s}}{T}\right), \quad (\text{A.8})$$

where $s_{\min} = \max[(m_X + m_a)^2, (m_i + m_j)^2]$. Here $\hat{\sigma}$ is the reduced cross section given by

$$\hat{\sigma}(Xa \rightarrow ij) = \frac{1}{8\pi s} \int_{t^-}^{t^+} dt |\mathcal{M}(Xa \rightarrow ij)|^2, \quad (\text{A.9})$$

with the integration limits

$$t^\pm = \frac{1}{4s} (m_X^2 - m_a^2 - m_i^2 + m_j^2)^2 - \frac{1}{4s} \left(\lambda^{1/2}(s, m_X^2, m_a^2) \mp \lambda^{1/2}(s, m_i^2, m_j^2) \right)^2 \quad (\text{A.10})$$

where $\lambda(x, y, z) = x^2 + y^2 + z^2 - 2xy - 2xz - 2yz$ is the Källén function.

To apply this formalism to the leptoquark model given in Sec. 2 we make the replacement $X \rightarrow S_1, S_1^*$, and identify the relevant decay- and scattering processes as those shown in Figs 2 and 3. Using Eq. A.1 we then have

$$zHn_\gamma \frac{d\eta_{S_1}}{dz} = -D - D_0, \quad (\text{A.11})$$

$$zHn_\gamma \frac{d\eta_{S_1^*}}{dz} = -\bar{D} - \bar{D}_0, \quad (\text{A.12})$$

where

$$D \equiv \gamma_D \left[(r + \epsilon) \frac{\eta_{S_1}^{\text{eq}}}{\eta_{S_1}} - (r - \epsilon) \frac{\eta_H \eta_{\tilde{R}_2^\dagger}}{\eta_H^{\text{eq}} \eta_{\tilde{R}_2^\dagger}^{\text{eq}}} \right], \quad (\text{A.13})$$

$$D_0 \equiv \gamma_D \left[(1 - r - \epsilon) \frac{\eta_{S_1}^{\text{eq}}}{\eta_{S_1}} - (1 - r + \epsilon) \frac{\eta_{\tilde{L}} \eta_{\tilde{Q}}}{\eta_L^{\text{eq}} \eta_Q^{\text{eq}}} \right], \quad (\text{A.14})$$

$$\bar{D} \equiv \gamma_D \left[(r - \epsilon) \frac{\eta_{S_1^*}^{\text{eq}}}{\eta_{S_1^*}} - (r + \epsilon) \frac{\eta_{H^\dagger} \eta_{\tilde{R}_2}}{\eta_H^{\text{eq}} \eta_{\tilde{R}_2}^{\text{eq}}} \right], \quad (\text{A.15})$$

$$\bar{D}_0 \equiv \gamma_D \left[(1 - r + \epsilon) \frac{\eta_{S_1^*}^{\text{eq}}}{\eta_{S_1^*}} - (1 - r - \epsilon) \frac{\eta_{\tilde{L}} \eta_Q}{\eta_L^{\text{eq}} \eta_Q^{\text{eq}}} \right]. \quad (\text{A.16})$$

Here r and ϵ are given in terms of the branching ratios of S_1 and S_1^* as

$$r \equiv \text{BR}(S_1 \rightarrow H\tilde{R}_2^\dagger) + \text{BR}(S_1^* \rightarrow H^\dagger\tilde{R}_2) \quad (\text{A.17})$$

$$\epsilon \equiv \text{BR}(S_1 \rightarrow H\tilde{R}_2^\dagger) - \text{BR}(S_1^* \rightarrow H^\dagger\tilde{R}_2) \quad (\text{A.18})$$

and the total decay rate γ_D is given by

$$\gamma_D \equiv \gamma_{\text{tree}}^{\text{eq}}(S_1 \rightarrow H\tilde{R}_2^\dagger) + \gamma_{\text{tree}}^{\text{eq}}(S_1 \rightarrow \bar{L}\bar{Q}), \quad (\text{A.19})$$

where $\gamma_{\text{tree}}^{\text{eq}}$ is the tree-level decay rate. For convenience we define

$$\eta_{S_1^+} \equiv \frac{1}{2}(\eta_{S_1} + \eta_{S_1^*}), \quad (\text{A.20})$$

$$\eta_{S_1^-} \equiv \frac{1}{2}(\eta_{S_1} - \eta_{S_1^*}), \quad (\text{A.21})$$

such that

$$zHn_\gamma \frac{d\eta_{S_1^+}}{dz} = -\frac{1}{2}(D + \bar{D} + D_0 + \bar{D}_0), \quad (\text{A.22})$$

$$zHn_\gamma \frac{d\eta_{S_1^-}}{dz} = -\frac{1}{2}(D - \bar{D} + D_0 - \bar{D}_0). \quad (\text{A.23})$$

Next, we use chemical potential relations to rewrite the number densities of the light particles H , \tilde{R}_2^\dagger , Q , and L in terms of the $B-L$ number density. To do this we begin by writing the number density n_a of a particle a in thermal equilibrium as [51]

$$n_a = \frac{g_a T^3}{\pi^2} \times \begin{cases} \zeta(3) + \frac{\mu_a}{T}\zeta(2) + \dots & (\text{boson}) \\ \frac{3}{4}\zeta(3) + \frac{\mu_a}{T}\frac{\zeta(2)}{2} + \dots & (\text{fermion}) \end{cases}, \quad (\text{A.24})$$

where μ_a is the chemical potential, which we have assumed to be small, $\mu_a/T \ll 1$. Note that we have the relation $\mu_a = -\mu_{\bar{a}}$ for antiparticle \bar{a} . We now wish to relate the different chemical potentials to each other using the fact that some interactions are in chemical equilibrium in the early Universe. In the SM we have the three Yukawa interactions

$$\mu_{q_i} = \mu_{\bar{u}_i^c} - \mu_H, \quad \mu_{q_i} = \mu_{\bar{d}_i^c} + \mu_H, \quad \mu_{L_i} = \mu_{\bar{e}_i^c} + \mu_H, \quad (\text{A.25})$$

and electroweak sphaleron

$$\sum_i \mu_{q_i} = -\frac{1}{3} \sum_i \mu_{L_i}, \quad (\text{A.26})$$

where i denotes the generation. For the benchmark scenario chosen in Sec. 5 using the leptoquark model presented in Sec. 2 we can also assume that the reaction $\tilde{R}_2^\dagger \leftrightarrow L + \bar{d}$ is in equilibrium, which lets us write

$$\mu_{\tilde{R}_2^\dagger} = \mu_{L_i} - \mu_{\bar{d}_i^c}. \quad (\text{A.27})$$

Further requiring a vanishing total $U(1)_Y$ hypercharge lets us write

$$0 = \sum_i Q_i^{U(1)_Y} (n_i - \bar{n}_i), \quad (\text{A.28})$$

where $Q_i^{U(1)_Y}$ is the $U(1)_Y$ charge of particle i , and the sum goes over all particle species that are in thermal equilibrium. We then relate the different chemical potentials to that of \tilde{R}_2^\dagger ,

$$\mu_a \equiv x_a \mu_{\tilde{R}_2^\dagger}. \quad (\text{A.29})$$

Next, we want to express $\mu_{\tilde{R}_2}$ in terms of the $B - L$ number density $n_{\Delta(B-L)}$ given by

$$n_{\Delta(B-L)} \equiv n_{B-L} - n_{\bar{B}-\bar{L}} = \sum_i Q_i^{B-L} (n_i - \bar{n}_i), \quad (\text{A.30})$$

and we further relate $\mu_{\tilde{R}_2^\dagger}$ to the $B - L$ density

$$\frac{\eta_{\Delta(B-L)}}{\eta_{B-L}^{\text{eq}}} \equiv C_{\tilde{R}_2^\dagger} \frac{\zeta(2)}{\zeta(3)} \frac{\mu_{\tilde{R}_2^\dagger}}{T}, \quad (\text{A.31})$$

where explicitly we have

$$C_{\tilde{R}_2^\dagger} = \frac{192 - (12 - 68x_L)N}{96 - 9N}, \quad (\text{A.32})$$

where N is the number of fermion families. The Boltzmann equations in Eqs. (A.22) and (A.23) can now be written as

$$zHn_\gamma \frac{d\eta_{S_1^+}}{dz} = -\gamma_D \left[\frac{\eta_{S_1^+}}{\eta_{S_1}^{\text{eq}}} - 1 + \frac{\epsilon}{2} \frac{x_H + 1 + \frac{2}{3}(x_L + x_Q)}{C_{\tilde{R}_2^\dagger}} \frac{\eta_{\Delta(B-L)}}{\eta_{B-L}^{\text{eq}}} \right], \quad (\text{A.33})$$

$$zHn_\gamma \frac{d\eta_{S_1^-}}{dz} = -\gamma_D \left[\frac{\eta_{S_1^-}}{\eta_{S_1}^{\text{eq}}} - \frac{\frac{r}{2}(x_H + 1) - \frac{1}{3}(2 - r)(x_L + x_Q)}{C_{\tilde{R}_2^\dagger}} \frac{\eta_{\Delta(B-L)}}{\eta_{B-L}^{\text{eq}}} \right]. \quad (\text{A.34})$$

The corresponding equation for $\eta_{\Delta(B-L)}$ can be expressed in terms of $\eta_{\tilde{R}_2^\dagger}$ using Eqs. (A.24) and (A.31) such that

$$zHn_\gamma \frac{d\eta_{\Delta(B-L)}}{dz} = \frac{\eta_{B-L}^{\text{eq}}}{2\eta_{\tilde{R}_2^\dagger}^{\text{eq}}} C_{\tilde{R}_2^\dagger} zHn_\gamma \left(\frac{d\eta_{\tilde{R}_2^\dagger}}{dz} - \frac{d\eta_{\tilde{R}_2}}{dz} \right). \quad (\text{A.35})$$

The equations for \tilde{R}_2^\dagger and \tilde{R}_2 are in turn given by

$$zHn_\gamma \frac{d\eta_{\tilde{R}_2^\dagger}}{dz} = D - S - 2T_A - 2T_B \quad (\text{A.36})$$

$$zHn_\gamma \frac{d\eta_{\tilde{R}_2}}{dz} = \bar{D} - \bar{S} - 2\bar{T}_A - 2\bar{T}_B. \quad (\text{A.37})$$

Here S and \bar{S} correspond to s -channel two-to-two scattering processes, and T_i and \bar{T}_i for

$i \in \{A, B\}$ similarly correspond to t -channel diagrams (c.f. Fig. 3), where the factor 2 accounts for the u -channel. The s -channel terms are given by

$$S \equiv \gamma_{\text{sub}}^{\text{eq}}(H\tilde{R}_2^\dagger \rightarrow \bar{L}\bar{Q}) \frac{\eta_H \eta_{\tilde{R}_2^\dagger}}{\eta_H^{\text{eq}} \eta_{\tilde{R}_2^\dagger}^{\text{eq}}} - \gamma_{\text{sub}}^{\text{eq}}(\bar{L}\bar{Q} \rightarrow H\tilde{R}_2^\dagger) \frac{\eta_{\bar{L}} \eta_{\bar{Q}}}{\eta_L^{\text{eq}} \eta_Q^{\text{eq}}}, \quad (\text{A.38})$$

$$\bar{S} \equiv \gamma_{\text{sub}}^{\text{eq}}(H^\dagger \tilde{R}_2 \rightarrow LQ) \frac{\eta_{H^\dagger} \eta_{\tilde{R}_2}}{\eta_H^{\text{eq}} \eta_{\tilde{R}_2}^{\text{eq}}} - \gamma_{\text{sub}}^{\text{eq}}(Lq \rightarrow H^\dagger \tilde{R}_2) \frac{\eta_L \eta_Q}{\eta_L^{\text{eq}} \eta_Q^{\text{eq}}}, \quad (\text{A.39})$$

where $\gamma_{\text{sub}}^{\text{eq}}$ is the s -channel reaction rate with the on-shell contribution subtracted

$$\gamma_{\text{sub}}^{\text{eq}}(Xa \rightarrow ij) \equiv \gamma^{\text{eq}}(Xa \rightarrow ij) - \gamma_{\text{on-shell}}^{\text{eq}}(Xa \rightarrow ij). \quad (\text{A.40})$$

This subtraction is done in order to avoid double counting of the decay- and inverse decay processes. The relevant on-shell contributions can be written in terms of the decay reaction rate, e.g.

$$\begin{aligned} \gamma_{\text{on-shell}}^{\text{eq}}(H\tilde{R}_2^\dagger \rightarrow \bar{L}\bar{Q}) &= \gamma^{\text{eq}}(H\tilde{R}_2^\dagger \rightarrow S_1) \text{BR}(S_1 \rightarrow \bar{L}\bar{Q}) \\ &= \gamma^{\text{eq}}(S_1^* \rightarrow H^\dagger \tilde{R}_2) \text{BR}(S_1 \rightarrow \bar{L}\bar{Q}), \end{aligned} \quad (\text{A.41})$$

where in the last step we used CPT invariance. We then find

$$\gamma_{\text{on-shell}}^{\text{eq}}(H\tilde{R}_2^\dagger \rightarrow \bar{L}\bar{Q}) \approx \frac{\gamma_D}{2} \left(r - \frac{r^2}{2} - \epsilon \right), \quad (\text{A.42})$$

$$\gamma_{\text{on-shell}}^{\text{eq}}(\bar{L}\bar{Q} \rightarrow H\tilde{R}_2^\dagger) \approx \frac{\gamma_D}{2} \left(r - \frac{r^2}{2} + \epsilon \right), \quad (\text{A.43})$$

$$\gamma_{\text{on-shell}}^{\text{eq}}(H^\dagger \tilde{R}_2 \rightarrow LQ) \approx \frac{\gamma_D}{2} \left(r - \frac{r^2}{2} + \epsilon \right), \quad (\text{A.44})$$

$$\gamma_{\text{on-shell}}^{\text{eq}}(Lq \rightarrow H^\dagger \tilde{R}_2) \approx \frac{\gamma_D}{2} \left(r - \frac{r^2}{2} - \epsilon \right). \quad (\text{A.45})$$

Here we have included CP -violating effects in the on-shell component that we subtract up to linear order in ϵ , in order to remain consistent with the decay rate relations. However, we may safely neglect CP -violation in the full reaction rate without encountering inconsistencies, which we will do for simplicity by defining

$$\gamma_S \equiv \gamma^{\text{eq}}(H\tilde{R}_2^\dagger \rightarrow \bar{L}\bar{Q}) = \gamma^{\text{eq}}(H^\dagger \tilde{R}_2 \rightarrow LQ). \quad (\text{A.46})$$

This leads to

$$S = \left[\gamma_S - \frac{\gamma_D}{2} \left(r - \frac{r^2}{2} - \epsilon \right) \right] \frac{\eta_H \eta_{\tilde{R}_2^\dagger}}{\eta_H^{\text{eq}} \eta_{\tilde{R}_2^\dagger}^{\text{eq}}} - \left[\gamma_S - \frac{\gamma_D}{2} \left(r - \frac{r^2}{2} - \epsilon \right) \right] \frac{\eta_{\bar{L}} \eta_{\bar{Q}}}{\eta_L^{\text{eq}} \eta_Q^{\text{eq}}}, \quad (\text{A.47})$$

$$\bar{S} = \left[\gamma_S - \frac{\gamma_D}{2} \left(r - \frac{r^2}{2} - \epsilon \right) \right] \frac{\eta_{H^\dagger} \eta_{\tilde{R}_2}}{\eta_H^{\text{eq}} \eta_{\tilde{R}_2}^{\text{eq}}} - \left[\gamma_S - \frac{\gamma_D}{2} \left(r - \frac{r^2}{2} - \epsilon \right) \right] \frac{\eta_L \eta_Q}{\eta_L^{\text{eq}} \eta_Q^{\text{eq}}}. \quad (\text{A.48})$$

For the t -channel terms we have

$$T_A = \gamma_{T_A} \left(\frac{\eta_{\tilde{R}_2^\dagger} \eta_Q}{\eta_{\tilde{R}_2^\dagger}^{\text{eq}} \eta_Q^{\text{eq}}} - \frac{\eta_{H^\dagger} \eta_{\bar{L}}}{\eta_H^{\text{eq}} \eta_L^{\text{eq}}} \right), \quad (\text{A.49})$$

$$T_B = \gamma_{T_B} \left(\frac{\eta_{\tilde{R}_2^\dagger} \eta_L}{\eta_{\tilde{R}_2^\dagger}^{\text{eq}} \eta_L^{\text{eq}}} - \frac{\eta_{H^\dagger} \eta_{\bar{Q}}}{\eta_H^{\text{eq}} \eta_Q^{\text{eq}}} \right), \quad (\text{A.50})$$

$$\overline{T_A} = \gamma_{T_A} \left(\frac{\eta_{\tilde{R}_2} \eta_{\bar{Q}}}{\eta_{\tilde{R}_2}^{\text{eq}} \eta_Q^{\text{eq}}} - \frac{\eta_H \eta_L}{\eta_H^{\text{eq}} \eta_L^{\text{eq}}} \right), \quad (\text{A.51})$$

$$\overline{T_B} = \gamma_{T_B} \left(\frac{\eta_{\tilde{R}_2} \eta_{\bar{L}}}{\eta_{\tilde{R}_2}^{\text{eq}} \eta_L^{\text{eq}}} - \frac{\eta_H \eta_Q}{\eta_H^{\text{eq}} \eta_Q^{\text{eq}}} \right), \quad (\text{A.52})$$

where we have again assumed CP -conservation for simplicity, such that

$$\gamma_{T_A} \equiv \gamma^{\text{eq}}(\tilde{R}_2^\dagger q \rightarrow H^\dagger \bar{L}) = \gamma^{\text{eq}}(\tilde{R}_2 \bar{Q} \rightarrow HL), \quad (\text{A.53})$$

$$\gamma_{T_B} \equiv \gamma^{\text{eq}}(\tilde{R}_2^\dagger L \rightarrow H^\dagger \bar{Q}) = \gamma^{\text{eq}}(\tilde{R}_2 \bar{L} \rightarrow HQ). \quad (\text{A.54})$$

We now find

$$\begin{aligned} z H n_\gamma \frac{d\eta_{\Delta(B-L)}}{dz} &= \frac{\eta_{B-L}^{\text{eq}}}{\eta_{\tilde{R}_2^\dagger}^{\text{eq}}} \left\{ C_{\tilde{R}_2^\dagger} \frac{\gamma_D}{2} \left[r \frac{\eta_{S_1^-}}{\eta_{S_1}^{\text{eq}}} + \epsilon \left(\frac{\eta_{S_1^+}}{\eta_{S_1}^{\text{eq}}} - 1 \right) \right] \right. \\ &\quad \left. - r \frac{\gamma_D}{2} \left[\frac{r}{2} (x_H + 1) - \frac{1}{3} (2 - r) (x_L + x_Q) \right] \frac{\eta_{\Delta(B-L)}}{\eta_{B-L}^{\text{eq}}} \right. \\ &\quad \left. - \left(x_H + 1 + \frac{2}{3} (x_L + x_Q) \right) (\gamma_S + 2\gamma_{T_A} + 2\gamma_{T_B}) \frac{\eta_{\Delta(B-L)}}{\eta_{B-L}^{\text{eq}}} \right\}. \end{aligned} \quad (\text{A.55})$$

Using the chemical potential relations we see that we only need to find x_L , which is given by

$$x_L = \frac{3N}{6N + 2}. \quad (\text{A.56})$$

This lets us write our set of three Boltzmann equations as

$$z H n_\gamma \frac{d\eta_{S_1^+}}{dz} = -\gamma_D \left[\frac{\eta_{S_1^+}}{\eta_{S_1}^{\text{eq}}} - 1 + \epsilon \frac{1 - \frac{4}{9} x_L}{C_{\tilde{R}_2^\dagger}} \frac{\eta_{\Delta(B-L)}}{\eta_{B-L}^{\text{eq}}} \right], \quad (\text{A.57})$$

$$z H n_\gamma \frac{d\eta_{S_1^-}}{dz} = -\gamma_D \left[\frac{\eta_{S_1^-}}{\eta_{S_1}^{\text{eq}}} - \frac{r - \frac{4}{9} x_L (1 + r)}{C_{\tilde{R}_2^\dagger}} \frac{\eta_{\Delta(B-L)}}{\eta_{B-L}^{\text{eq}}} \right], \quad (\text{A.58})$$

and

$$zHn_\gamma \frac{d\eta_{\Delta(B-L)}}{dz} = \frac{\eta_{B-L}^{\text{eq}}}{\eta_{\tilde{R}_2^\dagger}^{\text{eq}}} \left\{ C_{\tilde{R}_2^\dagger} \frac{\gamma_D}{2} \left[r \frac{\eta_{S_1^-}^{\text{eq}}}{\eta_{S_1}^{\text{eq}}} + \epsilon \left(\frac{\eta_{S_1^+}^{\text{eq}}}{\eta_{S_1}^{\text{eq}}} - 1 \right) \right] \right. \\ \left. - \left[r \frac{\gamma_D}{2} \left(r - \frac{4}{9} x_L (1+r) \right) + \gamma_W \left(1 - \frac{4}{9} x_L \right) \right] \frac{\eta_{\Delta(B-L)}^{\text{eq}}}{\eta_{B-L}^{\text{eq}}} \right\}, \quad (\text{A.59})$$

where

$$\gamma_W \equiv \gamma_S + 2\gamma_{T_A} + 2\gamma_{T_B}. \quad (\text{A.60})$$

Defining

$$c_+ \equiv \frac{1 - \frac{4}{9} x_L}{C_{\tilde{R}_2^\dagger}}, \quad c_- \equiv \frac{r - \frac{4}{9} x_L (1+r)}{C_{\tilde{R}_2^\dagger}}, \quad c_{\Delta(B-L)} \equiv \frac{\eta_{B-L}^{\text{eq}}}{\eta_{\tilde{R}_2^\dagger}^{\text{eq}}} C_{\tilde{R}_2^\dagger}, \quad (\text{A.61})$$

we finally have

$$zHn_\gamma \frac{d\eta_{S_1^+}^{\text{eq}}}{dz} = -\gamma_D \left[\frac{\eta_{S_1^+}^{\text{eq}}}{\eta_{S_1}^{\text{eq}}} - 1 + \epsilon c_+ \frac{\eta_{\Delta(B-L)}}{\eta_{B-L}^{\text{eq}}} \right], \quad (\text{A.62})$$

$$zHn_\gamma \frac{d\eta_{S_1^-}^{\text{eq}}}{dz} = -\gamma_D \left[\frac{\eta_{S_1^-}^{\text{eq}}}{\eta_{S_1}^{\text{eq}}} - c_- \frac{\eta_{\Delta(B-L)}}{\eta_{B-L}^{\text{eq}}} \right], \quad (\text{A.63})$$

$$\frac{zHn_\gamma}{c_{\Delta(B-L)}} \frac{d\eta_{\Delta(B-L)}}{dz} = \frac{\gamma_D}{2} \left[r \frac{\eta_{S_1^-}^{\text{eq}}}{\eta_{S_1}^{\text{eq}}} + \epsilon \left(\frac{\eta_{S_1^+}^{\text{eq}}}{\eta_{S_1}^{\text{eq}}} - 1 \right) \right] - \left(c_- r \frac{\gamma_D}{2} + c_+ \gamma_W \right) \frac{\eta_{\Delta(B-L)}}{\eta_{B-L}^{\text{eq}}}. \quad (\text{A.64})$$

References

- [1] PLANCK collaboration, N. Aghanim et al., *Planck 2018 results. VI. Cosmological parameters*, *Astron. Astrophys.* **641** (2020) A6, [[1807.06209](#)].
- [2] SUPER-KAMIOKANDE collaboration, Y. Fukuda et al., *Evidence for oscillation of atmospheric neutrinos*, *Phys. Rev. Lett.* **81** (1998) 1562–1567, [[hep-ex/9807003](#)].
- [3] SNO collaboration, Q. R. Ahmad et al., *Direct evidence for neutrino flavor transformation from neutral current interactions in the Sudbury Neutrino Observatory*, *Phys. Rev. Lett.* **89** (2002) 011301, [[nucl-ex/0204008](#)].
- [4] S. Y. Khlebnikov and M. E. Shaposhnikov, *The Statistical Theory of Anomalous Fermion Number Nonconservation*, *Nucl. Phys. B* **308** (1988) 885–912.
- [5] P. Minkowski, $\mu \rightarrow e\gamma$ at a Rate of One Out of 10^9 Muon Decays?, *Phys. Lett. B* **67** (1977) 421–428.
- [6] T. Yanagida, *Horizontal gauge symmetry and masses of neutrinos*, *Conf. Proc. C* **7902131** (1979) 95–99.
- [7] M. Gell-Mann, P. Ramond and R. Slansky, *Complex Spinors and Unified Theories*, *Conf. Proc. C* **790927** (1979) 315–321, [[1306.4669](#)].
- [8] R. N. Mohapatra and G. Senjanovic, *Neutrino Masses and Mixings in Gauge Models with Spontaneous Parity Violation*, *Phys. Rev. D* **23** (1981) 165.

- [9] S. Davidson and A. Ibarra, *A Lower bound on the right-handed neutrino mass from leptogenesis*, *Phys. Lett. B* **535** (2002) 25–32, [[hep-ph/0202239](#)].
- [10] M. Fukugita and T. Yanagida, *Baryogenesis Without Grand Unification*, *Phys. Lett. B* **174** (1986) 45–47.
- [11] A. Pilaftsis and T. E. J. Underwood, *Resonant leptogenesis*, *Nucl. Phys. B* **692** (2004) 303–345, [[hep-ph/0309342](#)].
- [12] A. Zee, *A Theory of Lepton Number Violation, Neutrino Majorana Mass, and Oscillation*, *Phys. Lett. B* **93** (1980) 389.
- [13] Z.-j. Tao, *Radiative seesaw mechanism at weak scale*, *Phys. Rev. D* **54** (1996) 5693–5697, [[hep-ph/9603309](#)].
- [14] E. Ma, *Pathways to naturally small neutrino masses*, *Phys. Rev. Lett.* **81** (1998) 1171–1174, [[hep-ph/9805219](#)].
- [15] E. Ma, *Verifiable radiative seesaw mechanism of neutrino mass and dark matter*, *Phys. Rev. D* **73** (2006) 077301, [[hep-ph/0601225](#)].
- [16] Y. Cai, J. Herrero-García, M. A. Schmidt, A. Vicente and R. R. Volkas, *From the trees to the forest: a review of radiative neutrino mass models*, *Front. in Phys.* **5** (2017) 63, [[1706.08524](#)].
- [17] C.-K. Chua, X.-G. He and W.-Y. P. Hwang, *Neutrino mass induced radiatively by supersymmetric leptoquarks*, *Phys. Lett. B* **479** (2000) 224–229, [[hep-ph/9905340](#)].
- [18] U. Mahanta, *Neutrino masses and mixing angles from leptoquark interactions*, *Phys. Rev. D* **62** (2000) 073009, [[hep-ph/9909518](#)].
- [19] D. Aristizabal Sierra, M. Hirsch and S. G. Kovalenko, *Leptoquarks: Neutrino masses and accelerator phenomenology*, *Phys. Rev. D* **77** (2008) 055011, [[0710.5699](#)].
- [20] I. Doršner, S. Fajfer and N. Košnik, *Leptoquark mechanism of neutrino masses within the grand unification framework*, *Eur. Phys. J. C* **77** (2017) 417, [[1701.08322](#)].
- [21] O. Catà and T. Mannel, *Linking lepton number violation with B anomalies*, [1903.01799](#).
- [22] K. S. Babu, P. S. B. Dev, S. Jana and A. Thapa, *Non-Standard Interactions in Radiative Neutrino Mass Models*, *JHEP* **03** (2020) 006, [[1907.09498](#)].
- [23] F. F. Deppisch, K. Fridell and J. Harz, *Constraining lepton number violating interactions in rare kaon decays*, *JHEP* **12** (2020) 186, [[2009.04494](#)].
- [24] S. Fajfer, L. P. S. Leal, O. Sumensari and R. Z. Funchal, *Correlating $0\nu\beta\beta$ decays and flavor observables in leptoquark models*, [2406.20050](#).
- [25] P. S. B. Dev, S. Goswami, C. Majumdar and D. Pachhar, *Neutrinoless Double Beta Decay from Scalar Leptoquarks: Interplay with Neutrino Mass and Flavor Physics*, [2407.04670](#).
- [26] W. Buchmuller, R. Ruckl and D. Wyler, *Leptoquarks in Lepton - Quark Collisions*, *Phys. Lett. B* **191** (1987) 442–448.
- [27] M. Hirsch, H. V. Klapdor-Kleingrothaus and S. G. Kovalenko, *New low-energy leptoquark interactions*, *Phys. Lett. B* **378** (1996) 17–22, [[hep-ph/9602305](#)].
- [28] M. Hirsch, H. V. Klapdor-Kleingrothaus and S. G. Kovalenko, *New leptoquark mechanism of neutrinoless double beta decay*, *Phys. Rev. D* **54** (1996) R4207–R4210, [[hep-ph/9603213](#)].

- [29] E. Ma, M. Raidal and U. Sarkar, *Baryogenesis with scalar bilinears*, *Phys. Rev. D* **60** (1999) 076005, [[hep-ph/9811240](#)].
- [30] K. S. Babu and R. N. Mohapatra, *B-L Violating Nucleon Decay and GUT Scale Baryogenesis in $SO(10)$* , *Phys. Rev. D* **86** (2012) 035018, [[1203.5544](#)].
- [31] K. S. Babu and R. N. Mohapatra, *B-L Violating Proton Decay Modes and New Baryogenesis Scenario in $SO(10)$* , *Phys. Rev. Lett.* **109** (2012) 091803, [[1207.5771](#)].
- [32] C. Hati and U. Sarkar, *$B - L$ violating nucleon decays as a probe of leptiquarks and implications for baryogenesis*, *Nucl. Phys. B* **954** (2020) 114985, [[1805.06081](#)].
- [33] T. Blažek, J. Heeck, J. Heisig, P. Maták and V. Zaujec, *Dirac leptogenesis from asymmetry wash-in via scatterings*, *Phys. Rev. D* **110** (2024) 055042, [[2404.16934](#)].
- [34] I. Doršner, S. Fajfer, A. Greljo, J. F. Kamenik and N. Košnik, *Physics of leptiquarks in precision experiments and at particle colliders*, *Phys. Rept.* **641** (2016) 1–68, [[1603.04993](#)].
- [35] A. de Gouvea and J. Jenkins, *A Survey of Lepton Number Violation Via Effective Operators*, *Phys. Rev. D* **77** (2008) 013008, [[0708.1344](#)].
- [36] L. Lehman, *Extending the Standard Model Effective Field Theory with the Complete Set of Dimension-7 Operators*, *Phys. Rev. D* **90** (2014) 125023, [[1410.4193](#)].
- [37] Y. Liao and X.-D. Ma, *Renormalization Group Evolution of Dimension-seven Baryon- and Lepton-number-violating Operators*, *JHEP* **11** (2016) 043, [[1607.07309](#)].
- [38] V. Cirigliano, W. Dekens, J. de Vries, M. L. Graesser and E. Mereghetti, *Neutrinoless double beta decay in chiral effective field theory: lepton number violation at dimension seven*, *JHEP* **12** (2017) 082, [[1708.09390](#)].
- [39] F. F. Deppisch, L. Graf, J. Harz and W.-C. Huang, *Neutrinoless Double Beta Decay and the Baryon Asymmetry of the Universe*, *Phys. Rev. D* **98** (2018) 055029, [[1711.10432](#)].
- [40] K. Fridell, L. Gráf, J. Harz and C. Hati, *Probing lepton number violation: a comprehensive survey of dimension-7 SMEFT*, *JHEP* **05** (2024) 154, [[2306.08709](#)].
- [41] K. Fridell, L. Gráf, J. Harz and C. Hati, *Radiative neutrino masses from dim-7 SMEFT: a simplified multi-scale approach*, [2412.14268](#).
- [42] I. Esteban, M. C. Gonzalez-Garcia, M. Maltoni, I. Martinez-Soler, J. a. P. Pinheiro and T. Schwetz, *NuFit-6.0: Updated global analysis of three-flavor neutrino oscillations*, [2410.05380](#).
- [43] KATRIN collaboration, M. Aker et al., *Direct neutrino-mass measurement based on 259 days of KATRIN data*, [2406.13516](#).
- [44] A. D. Sakharov, *Violation of CP Invariance, C asymmetry, and baryon asymmetry of the universe*, *Pisma Zh. Eksp. Teor. Fiz.* **5** (1967) 32–35.
- [45] G. D. Moore, *Sphaleron rate in the symmetric electroweak phase*, *Phys. Rev. D* **62** (2000) 085011, [[hep-ph/0001216](#)].
- [46] B. Garbrecht and P. Schwaller, *Spectator Effects during Leptogenesis in the Strong Washout Regime*, *JCAP* **10** (2014) 012, [[1404.2915](#)].
- [47] G. F. Giudice, A. Notari, M. Raidal, A. Riotto and A. Strumia, *Towards a complete theory of thermal leptogenesis in the SM and MSSM*, *Nucl. Phys. B* **685** (2004) 89–149, [[hep-ph/0310123](#)].

- [48] K. S. Babu and R. N. Mohapatra, *Coupling Unification, GUT-Scale Baryogenesis and Neutron-Antineutron Oscillation in $SO(10)$* , *Phys. Lett. B* **715** (2012) 328–334, [[1206.5701](#)].
- [49] S. Chongdar and S. Mishra, *Scalar triplet leptogenesis with a CP violating phase*, *Nucl. Phys. B* **995** (2023) 116346, [[2112.11838](#)].
- [50] K. Fridell, J. Harz and C. Hati, *Probing baryogenesis with neutron-antineutron oscillations*, *JHEP* **11** (2021) 185, [[2105.06487](#)].
- [51] J. A. Harvey and M. S. Turner, *Cosmological baryon and lepton number in the presence of electroweak fermion number violation*, *Phys. Rev. D* **42** (1990) 3344–3349.
- [52] J. Blumlein, E. Boos and A. Kryukov, *Leptoquark pair production in hadronic interactions*, *Z. Phys. C* **76** (1997) 137–153, [[hep-ph/9610408](#)].
- [53] I. Dorsner, S. Fajfer and A. Greljo, *Cornering Scalar Leptoquarks at LHC*, *JHEP* **10** (2014) 154, [[1406.4831](#)].
- [54] B. Diaz, M. Schmaltz and Y.-M. Zhong, *The leptoquark Hunter’s guide: Pair production*, *JHEP* **10** (2017) 097, [[1706.05033](#)].
- [55] M. Schmaltz and Y.-M. Zhong, *The leptoquark Hunter’s guide: large coupling*, *JHEP* **01** (2019) 132, [[1810.10017](#)].
- [56] P. Bandyopadhyay and R. Mandal, *Revisiting scalar leptoquark at the LHC*, *Eur. Phys. J. C* **78** (2018) 491, [[1801.04253](#)].
- [57] A. Greljo and N. Selimovic, *Lepton-Quark Fusion at Hadron Colliders, precisely*, *JHEP* **03** (2021) 279, [[2012.02092](#)].
- [58] I. Doršner, S. Fajfer and A. Lejlić, *Novel Leptoquark Pair Production at LHC*, *JHEP* **05** (2021) 167, [[2103.11702](#)].
- [59] A. Crivellin, M. Hoferichter, M. Kirk, C. A. Manzari and L. Schnell, *First-generation new physics in simplified models: from low-energy parity violation to the LHC*, *JHEP* **10** (2021) 221, [[2107.13569](#)].
- [60] A. Bhaskar, T. Mandal, S. Mitra and M. Sharma, *Improving third-generation leptoquark searches with combined signals and boosted top quarks*, *Phys. Rev. D* **104** (2021) 075037, [[2106.07605](#)].
- [61] A. Bhaskar, A. Das, T. Mandal, S. Mitra and R. Sharma, *Fresh look at the LHC limits on scalar leptoquarks*, *Phys. Rev. D* **109** (2024) 055018, [[2312.09855](#)].
- [62] N. Desai and A. Sengupta, *Status of leptoquark models after LHC Run-2 and discovery prospects at future colliders*, [2301.01754](#).
- [63] I. d. M. Varzielas and A. Sengupta, *Constraining flavoured leptoquarks with LHC and LFV*, *Nucl. Phys. B* **1001** (2024) 116495, [[2301.04119](#)].
- [64] ATLAS collaboration, G. Aad et al., *Search for pair production of third-generation leptoquarks decaying into a bottom quark and a τ -lepton with the ATLAS detector*, *Eur. Phys. J. C* **83** (2023) 1075, [[2303.01294](#)].
- [65] FCC collaboration, A. Abada et al., *FCC-ee: The Lepton Collider: Future Circular Collider Conceptual Design Report Volume 2*, *Eur. Phys. J. ST* **228** (2019) 261–623.
- [66] H. Pas, M. Hirsch, H. V. Klapdor-Kleingrothaus and S. G. Kovalenko, *Towards a superformula for neutrinoless double beta decay*, *Phys. Lett. B* **453** (1999) 194–198.

- [67] F. F. Deppisch, M. Hirsch and H. Pas, *Neutrinoless Double Beta Decay and Physics Beyond the Standard Model*, *J. Phys. G* **39** (2012) 124007, [[1208.0727](#)].
- [68] W. Rodejohann, *Neutrinoless double beta decay and neutrino physics*, *J. Phys. G* **39** (2012) 124008, [[1206.2560](#)].
- [69] L. Graf, F. F. Deppisch, F. Iachello and J. Kotila, *Short-Range Neutrinoless Double Beta Decay Mechanisms*, *Phys. Rev. D* **98** (2018) 095023, [[1806.06058](#)].
- [70] V. Cirigliano, W. Dekens, J. de Vries, M. L. Graesser and E. Mereghetti, *A neutrinoless double beta decay master formula from effective field theory*, *JHEP* **12** (2018) 097, [[1806.02780](#)].
- [71] F. F. Deppisch, L. Graf, F. Iachello and J. Kotila, *Analysis of light neutrino exchange and short-range mechanisms in $0\nu\beta\beta$ decay*, *Phys. Rev. D* **102** (2020) 095016, [[2009.10119](#)].
- [72] KAMLAND-ZEN collaboration, S. Abe et al., *Search for the Majorana Nature of Neutrinos in the Inverted Mass Ordering Region with KamLAND-Zen*, *Phys. Rev. Lett.* **130** (2023) 051801, [[2203.02139](#)].
- [73] T. Li, X.-D. Ma and M. A. Schmidt, *Implication of $K \rightarrow \pi\nu\bar{\nu}$ for generic neutrino interactions in effective field theories*, *Phys. Rev. D* **101** (2020) 055019, [[1912.10433](#)].
- [74] M. Gorbahn, U. Moldanazarova, K. H. Sieja, E. Stamou and M. Tabet, *The anatomy of $K^+ \rightarrow \pi^+\nu\bar{\nu}$ distributions*, *Eur. Phys. J. C* **84** (2024) 680, [[2312.06494](#)].
- [75] A. J. Buras, J. Harz and M. A. Mojahed, *Disentangling new physics in $K \rightarrow \pi\nu\bar{\nu}$ and $B \rightarrow K(K^*)\nu\bar{\nu}$ observables*, *JHEP* **10** (2024) 087, [[2405.06742](#)].
- [76] NA62 collaboration, E. Cortina Gil et al., *An investigation of the very rare $K^+ \rightarrow \pi^+\nu\bar{\nu}$ decay*, *JHEP* **11** (2020) 042, [[2007.08218](#)].
- [77] NA62 collaboration, E. Cortina Gil et al., *Measurement of the very rare $K^+ \rightarrow \pi^+\nu\bar{\nu}$ decay*, *JHEP* **06** (2021) 093, [[2103.15389](#)].
- [78] HIKE collaboration, E. Cortina Gil et al., *HIKE, High Intensity Kaon Experiments at the CERN SPS: Letter of Intent*, [2211.16586](#).
- [79] KOTO collaboration, H. Nanjo, *KOTO II at J-PARC : toward measurement of the branching ratio of $K_L \rightarrow \pi^0\nu\bar{\nu}$* , *J. Phys. Conf. Ser.* **2446** (2023) 012037.
- [80] BELLE-II collaboration, I. Adachi et al., *Evidence for $B^+ \rightarrow K^+\nu\bar{\nu}$ decays*, *Phys. Rev. D* **109** (2024) 112006, [[2311.14647](#)].
- [81] K. Fridell, M. Ghosh, T. Okui and K. Tobioka, *Decoding the $B \rightarrow K\nu\bar{\nu}$ excess at Belle II: Kinematics, operators, and masses*, *Phys. Rev. D* **109** (2024) 115006, [[2312.12507](#)].
- [82] P.-H. Gu and U. Sarkar, *Common Origin of Baryon Asymmetry and Proton Decay*, *Mod. Phys. Lett. A* **28** (2013) 1350159, [[1110.4581](#)].
- [83] I. Dorsner, S. Fajfer and N. Kosnik, *Heavy and light scalar leptoquarks in proton decay*, *Phys. Rev. D* **86** (2012) 015013, [[1204.0674](#)].
- [84] Y. Aoki, T. Izubuchi, E. Shintani and A. Soni, *Improved lattice computation of proton decay matrix elements*, *Phys. Rev. D* **96** (2017) 014506, [[1705.01338](#)].
- [85] RBC-UKQCD collaboration, Y. Aoki, P. Boyle, P. Cooney, L. Del Debbio, R. Kenway, C. M. Maynard et al., *Proton lifetime bounds from chirally symmetric lattice QCD*, *Phys. Rev. D* **78** (2008) 054505, [[0806.1031](#)].

- [86] SUPER-KAMIOKANDE collaboration, K. Abe et al., *Search for proton decay via $p \rightarrow e^+\pi^0$ and $p \rightarrow \mu^+\pi^0$ in 0.31 megaton-years exposure of the Super-Kamiokande water Cherenkov detector*, *Phys. Rev. D* **95** (2017) 012004, [[1610.03597](#)].
- [87] SUPER-KAMIOKANDE collaboration, K. Abe et al., *Search for Nucleon Decay via $n \rightarrow \bar{\nu}\pi^0$ and $p \rightarrow \bar{\nu}\pi^+$ in Super-Kamiokande*, *Phys. Rev. Lett.* **113** (2014) 121802, [[1305.4391](#)].
- [88] T.-K. Kuo and S. T. Love, *Neutron Oscillations and the Existence of Massive Neutral Leptons*, *Phys. Rev. Lett.* **45** (1980) 93.
- [89] R. N. Mohapatra and R. E. Marshak, *Local B-L Symmetry of Electroweak Interactions, Majorana Neutrinos and Neutron Oscillations*, *Phys. Rev. Lett.* **44** (1980) 1316–1319.
- [90] K. S. Babu, P. S. Bhupal Dev and R. N. Mohapatra, *Neutrino mass hierarchy, neutron - anti-neutron oscillation from baryogenesis*, *Phys. Rev. D* **79** (2009) 015017, [[0811.3411](#)].
- [91] SINDRUM II collaboration, W. H. Bertl et al., *A Search for muon to electron conversion in muonic gold*, *Eur. Phys. J. C* **47** (2006) 337–346.
- [92] P. W. Angel, N. L. Rodd and R. R. Volkas, *Origin of neutrino masses at the LHC: $\Delta L = 2$ effective operators and their ultraviolet completions*, *Phys. Rev. D* **87** (2013) 073007, [[1212.6111](#)].
- [93] Y. Cai, J. D. Clarke, M. A. Schmidt and R. R. Volkas, *Testing Radiative Neutrino Mass Models at the LHC*, *JHEP* **02** (2015) 161, [[1410.0689](#)].
- [94] R. Cepedello, M. Hirsch and J. C. Helo, *Loop neutrino masses from $d = 7$ operator*, *JHEP* **07** (2017) 079, [[1705.01489](#)].
- [95] J. de Blas, J. C. Criado, M. Perez-Victoria and J. Santiago, *Effective description of general extensions of the Standard Model: the complete tree-level dictionary*, *JHEP* **03** (2018) 109, [[1711.10391](#)].
- [96] J. Herrero-García and M. A. Schmidt, *Neutrino mass models: New classification and model-independent upper limits on their scale*, *Eur. Phys. J. C* **79** (2019) 938, [[1903.10552](#)].
- [97] U. Banerjee, J. Chakraborty, S. Prakash, S. U. Rahaman and M. Spannowsky, *Effective Operator Bases for Beyond Standard Model Scenarios: An EFT compendium for discoveries*, *JHEP* **01** (2021) 028, [[2008.11512](#)].
- [98] S. Das Bakshi, J. Chakraborty, S. Prakash, S. U. Rahaman and M. Spannowsky, *EFT diagrammatica: UV roots of the CP-conserving SMEFT*, *JHEP* **06** (2021) 033, [[2103.11593](#)].
- [99] M. Chala and A. Titov, *Neutrino masses in the Standard Model effective field theory*, *Phys. Rev. D* **104** (2021) 035002, [[2104.08248](#)].
- [100] K. K. Fridell, *Phenomenology of Baryogenesis and Neutrino Physics: From Effective Field Theory to Simplified Models*. PhD thesis, Munich, Tech. U., Technical University of Munich, 8, 2022.
- [101] F. C. Adams, *The degree of fine-tuning in our universe — and others*, *Phys. Rept.* **807** (2019) 1–111, [[1902.03928](#)].
- [102] M. Becker, K. Fridell, J. Harz and C. Hati, *Impact of Bound State Formation on Baryogenesis*, [2408.08361](#).